Science in China Series E: Technological Sciences

© 2008 SCIENCE IN CHINA PRESS
Springer

www.scichina.com
tech.scichina.com
www.springerlink.com

Review of zero-net-mass-flux jet and its application in separation flow control

ZHANG PanFeng, WANG JinJun† & FENG LiHao

Institute of Fluid Mechanics, Beijing University of Aeronautics and Astronautics, Beijing 100191,China

Since the zero-net-mass-flux (ZNMF) jet was first used as a laboratory flow control method in 1990's, it has attracted much attention. The ZNMF jet has unique features such as compact actuator, no requirement for external air supply, complex piping, etc., and becomes a hot topic research subject in fluid mechanics. This review introduces the state of the art in the development of ZNMF jet in the quiescent fluid, the interaction of the ZNMF jet with the cross flow and its application in the separation flow control. The evolution of the vortex ring/pair and the spacial flow structure of the ZNMF in quicent fluid or cross flow are presented, as well as the key parameter effects. At last, the applications of ZNMF jet in the wake control of the circular cylinder, the separation control on the airfoil and the aerodynamic force or moment control on MAV/UAV are presented.

zero-net-mass-flux jet, quiescent fluid, cross flow, separation control

1 Introduction

The zero-net-mass-flux (ZNMF) jet (also named as synthetic jets) was found by Ingard and Labate[1] in 1950, they used standing waves in an acoustically driven circular tube to induce an oscillating velocity field in the vicinity of an orifice endplate and observed the formation of the ZNMF jet from opposing trains of vortex rings on both sides of the orifice. In 1992, Ming et al.[2] found that a Helmholtz resonator could be excited by an inside sound source in the tube with resonant frequency, which is the most efficient energy transfer way from acoustic energy to fluid vibration energy. Then they used this new phenomenon of acoustic streaming as a separation flow control method. The ZNMF jet was first used as a laboratory flow control method by Wiltse and Glezer[3] in 1994, after that it attracted more and more attentions. Now, the ZNMF jet is a hot topic in fluid mechanics researches, and there are many universities and institutes in China that are conducting relative research work, including National University of Defense Technology[4−6],

Received October 25, 2007; accepted February 19, 2008
doi: 10.1007/s11431-008-0174-x
†Corresponding author (email: jjwang@buaa.edu.cn)
Supported by the National Natural Science Foundation of China (Grant No. 10425207) and the Aviation Creative Foundation of China (Grant No. 07A51001)

Beijing University of Aeronautics and Astronautics[7−11], Nanjing University of Aeronautics and Astronautics[2,12−14], Northwest Polytechnic University[15,16] and Tsinghua University[17,18]. Many reviews about this subject have been published[4,19]. Figure 1 presents the trends of the cited research article numbers by Science Cited Index (SCI) and Engineering Village (EI) in the last decade. It is apparent that the number of research articles about the ZNMF jet increases quickly and steadily, which indicates that the researchers have shown more interest in this research subject.

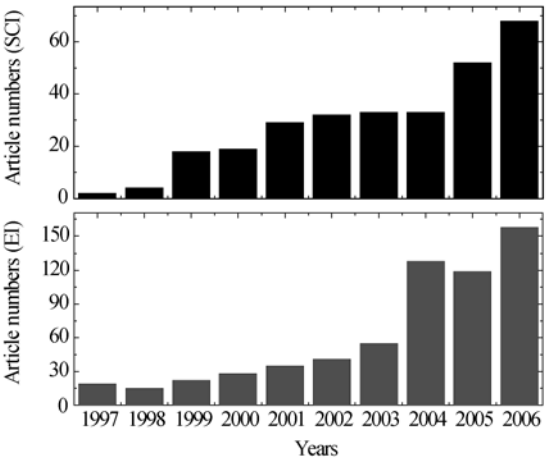

Figure 1 The article numbers about ZNMF jet cited by SCI/EI.

The ZNMF jet is usually produced by a sinusoidal oscillating membrane or piston to alternatively force fluid through an orifice into the external flow field and entrain fluid back. During the blowing stroke, the ejected fluid separates at the sharp edges of the orifice and rolls up to form a vortex pair or ring (2D with slot orifice and 3D with circular orifice, respectively). When the membrane begins its suction stroke, the vortex pair or ring is quite far from the orifice and keeps on propagating away due to its self-induced velocity. Hence, the vortex pair or ring would not be entrained back into the cavity, but it will coalesce to synthesize a jet with momentum transfer to the embedding flow (see Figure 2). The ZNMF jet has a unique feature compared with the traditional blowing or suction flow control methods, i.e. the ZNMF jet requires neither the external fluid supply nor the complex piping. This enables the ZNMF jet actuator to have some advantages such as reduced size and weight, improved manufacturability, low cost and increased reliability, so it is very popular worldwide as a flow control device nowadays. With the development of micro-electro-mechanical systems (MEMS)[3], the ZNMF jet actuator fabricated with MEMS technology will play a more important role in flow control of both external and internal flows[20].

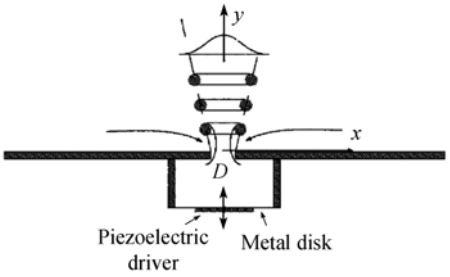

Figure 2 The sketch of the formation of ZNMF jet[22].

2 Development of ZNMF jet in quiescent flow

2.1 Key parameters of ZNMF jet actuator

For a typical ZNMF jet in quiescent flow, the vortex pair or ring formation and evolution depend on the following parameters: (1) the actuator scale parameters, which include the cavity diameter or width D (corresponding to the 3D circular and 2D slot jets, respectively), the cavity depth H, the circular orifice diameter or the slot orifice width D_0 and the orifice depth h; (2) the characteristic parameters of working fluid, which include the fluid density ρ and the kinematic viscosity μ; (3) the actuation parameters, which include the diaphragm oscillation amplitude Δ and the diaphragm oscillation frequency f. In order to simplify the key parameters which govern the characteristics of the ZNMF jet, Glezer and Amitay[21], and Smith and Glezer[22] proposed two independent dimen-

sionless parameters, the stroke length ratio and the Reynolds number based on the blowing stroke. According to the simple 'slug' model for vortex ring formation adopted by Glezer[23], the stroke length of the ZNMF jet represents the length of a fluid column containing the fluid that is pushed out of the orifice during the blowing stroke:

$$L_0 = U_0 T,$$

where T is the time period of actuator excitation and U_0 is the time-averaged blowing velocity over the entire period, i.e.

$$U_0 = \frac{1}{T}\int_0^{T/2} \tilde{u}_0(t)\mathrm{d}t,$$

where $\tilde{u}_0(t)$ is the instant stream-wise space averaged velocity over the orifice section. To compare the features of the ZNMF jet with the continuous jets, Smith and Glezer[22] introduced another dimensionless parameter, the stroke length ratio L, to describe the ZNMF jet. The stroke length ratio L is defined as

$$L=L_0/D_0.$$

It can be proved that L is linearly proportional to $\frac{\Delta}{D_0}\left(\frac{D}{D_0}\right)^2$ for actuators, when the flow in the actuator cavity can be regarded as incompressible. Therefore, the stroke length ratio L can represent the geometry characteristics of the actuator generally[24]. The Reynolds number of ZNMF is defined based on the actuator orifice D_0 and the time-averaged blowing velocity over the entire period U_0:

$$Re_{U_0} = \frac{U_0 D_0}{\nu}.$$

It could be drawn that the ZNMF jet is governed by the self induced velocity of the vortex formed during blowing stroke V_I and the averaged velocity during the suction stroke V_s according to its formation mechanism. When V_I/V_s is set larger than K (here K is a constant), the vortex pair formed in the bowing stroke would not be entrained back into the cavity in the suction stroke, which is the formation criterion for ZNMF jet. By order analysis of the magnitude, Utturkar et al.[25], and Holman et al.[26] gave the followings.

$$\frac{V_I}{V_s} \sim \frac{1}{St} = \frac{Re_{U_0}}{S^2} > K,$$

where $St = \frac{2\pi f D_0}{U_0} = \frac{2\pi}{L}$ is the Strouhal number and $S = \sqrt{\frac{2\pi f D_0^2}{\nu}} = \sqrt{\frac{2\pi Re_{U_0}}{L}}$ is the Stokes number. The data supports that the constant K is approximately 2.0 and 0.16 for two-dimensional and axisymmetrical ZNMF jets, respectively[26].

Since the stroke length ratio L represents the length of a fluid column containing the fluid that is pushed out of the orifice during the blowing stroke, the distance of the vortex pair or ring from the actuator orifice is determined by this parameter. If the stroke length ratio is too small, the vortex pair or ring formed during the bowing stroke is not far from the actuator orifice in the suction stroke, so it will be sucked back into the actuator cavity and not form the ZNMF jet with momentum export. In other way, the St number is proportional to the inverse of the stroke length ratio L, so the ZNMF jet formation criterion can be expressed as $\frac{1}{St} = \frac{L}{2\pi} > K$, which means the stroke length

ratio L also can be regarded as the domination parameter for ZNMF jet formation. Holman et al.[26] showed that the jet formation criterion becomes $L>0.50$ for the 2D slot ZNMF jet by theoretical analysis, which has some divergence for different orifice geometries. Shuster and Smith[27] obtained the same result by PIV experiments.

It is well know that the vortex pair or ring strength and location vary with the two key parameters mentioned above. Shuster and Smith[27] concluded that the distance of vortex pair or ring from the orifice increased with the stroke length ratio L through PIV experiments (as shown in Figure 3). They also argued that the vortex strength increased with the Reynolds number, but the location was not affected by the Reynolds number (as shown in Figure 4). Meanwhile, Smith and Glezer[22] obtained that the actual dimensional locations of the vortex pair varied with the Reynolds number in the range of $5.3<L<25$ and $104<Re_{U_0}<498$, but the dimensionless trajectories normalized by the stroke length L_0 of the vortex pair with different Reynolds numbers collapsed to the same curve. It is evident that the stroke length ratio determines the trajectory of the vortex pair or ring. After that, Smith and Swift[28] investigated the trajectory of the vortex pair with two key parameters varied in a larger range, and found that the trajectories normalized by stroke length were too close, but there was also some difference between them, which was caused by the transition phenomenon of the vortex pair or ring for the very large Reynolds number.

Although the circulation of the vortex pair or ring formed during the blowing stroke increases with the stroke length ratio L, when the stroke length ratio exceeds 4, the circulation in the primary vortex remains constant and the excess vorticity has to be shed in the form of secondary vortex trailing behind the primary vortex ring (as shown in Figure 5). Zhong et al.[24] showed the secondary vortex behind the primary vortex at L=7.1 by PIV in Figure 6. Shuster and Smith[27] also

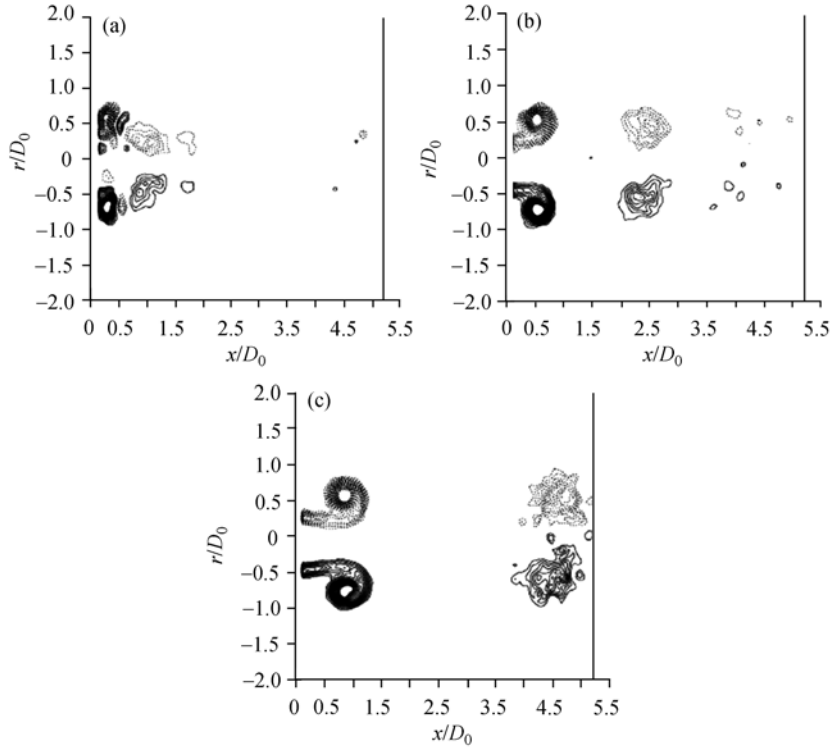

Figure 3 The contours of phase averaged vorticity produced by ZNMF jet with PIV measurement at phase angle 162°, Re_{U_0} =2500. (a) L=1.0; (b) L=2.0; (c) L=3.0[27].

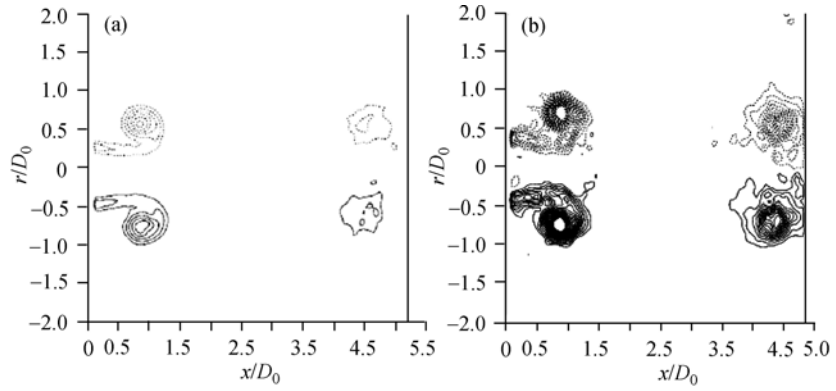

Figure 4 The contours of phase averaged vorticity produced by ZNMF jet with PIV measurement at phase angle 162°, L=3.0. (a) Re_{U_0}=2500; (b) Re_{U_0}=10000[27].

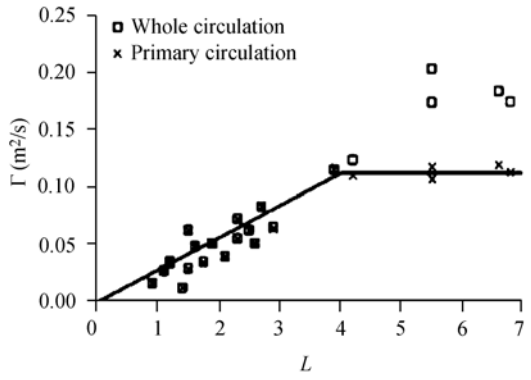

Figure 5 The total circulation and the circulation in the primary vortex ring with respect to the stroke length ratio[24].

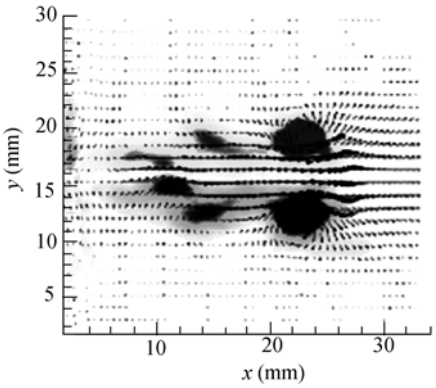

Figure 6 The secondary vortex behind the primary vortex ring, visualized by PIV[24].

obtained that the threshold of stroke length ratio L for the secondary vortex existence was 4—5 by the dye injection flow visualization, which is consistent with that of the pulsed jet[29].

The formation threshold of the ZNMF jet is that the self induced velocity of the vortex pair or ring formed during blowing stroke is larger than the averaged velocity during the suction stroke, so the vortex pair or ring formed during blowing stroke would not be entrained back into the cavity during suction stroke. Zhang and Wang[7] proposed a novel signal wave pattern to generate a more efficient ZNMF jet, which was realized by changing the suction duty cycle factor k (k=T_s/T_b, where T_s is the suction stroke period and T_b is the blowing stroke period), at the same time the two key parameters of the ZNMF jet defined above kept the same (the Reynolds number based on the time averaged blowing velocity and the stroke length ratio). Figure 7 shows vorticity contours during the blowing and suction strokes with suction duty cycle factors k=0.5, 1 and 2, respectively. The pictures in the left column are corresponding to the moment with the peak blowing velocity and the pictures in the right one are corresponding to the moment with the peak suction velocity. It is obvious that the position and scale of the first vortex pair formed near the edge of the orifice have little difference in the left column, but the position and scale of the secondary vortex pair at this moment increase with k, and the first vortex pair in the right column has the same behavior. It is evident that the variation of k does not affect the stroke length ratio, so the position of the vortex pair with different k during the blowing stroke has little difference. On the other hand, the efficient

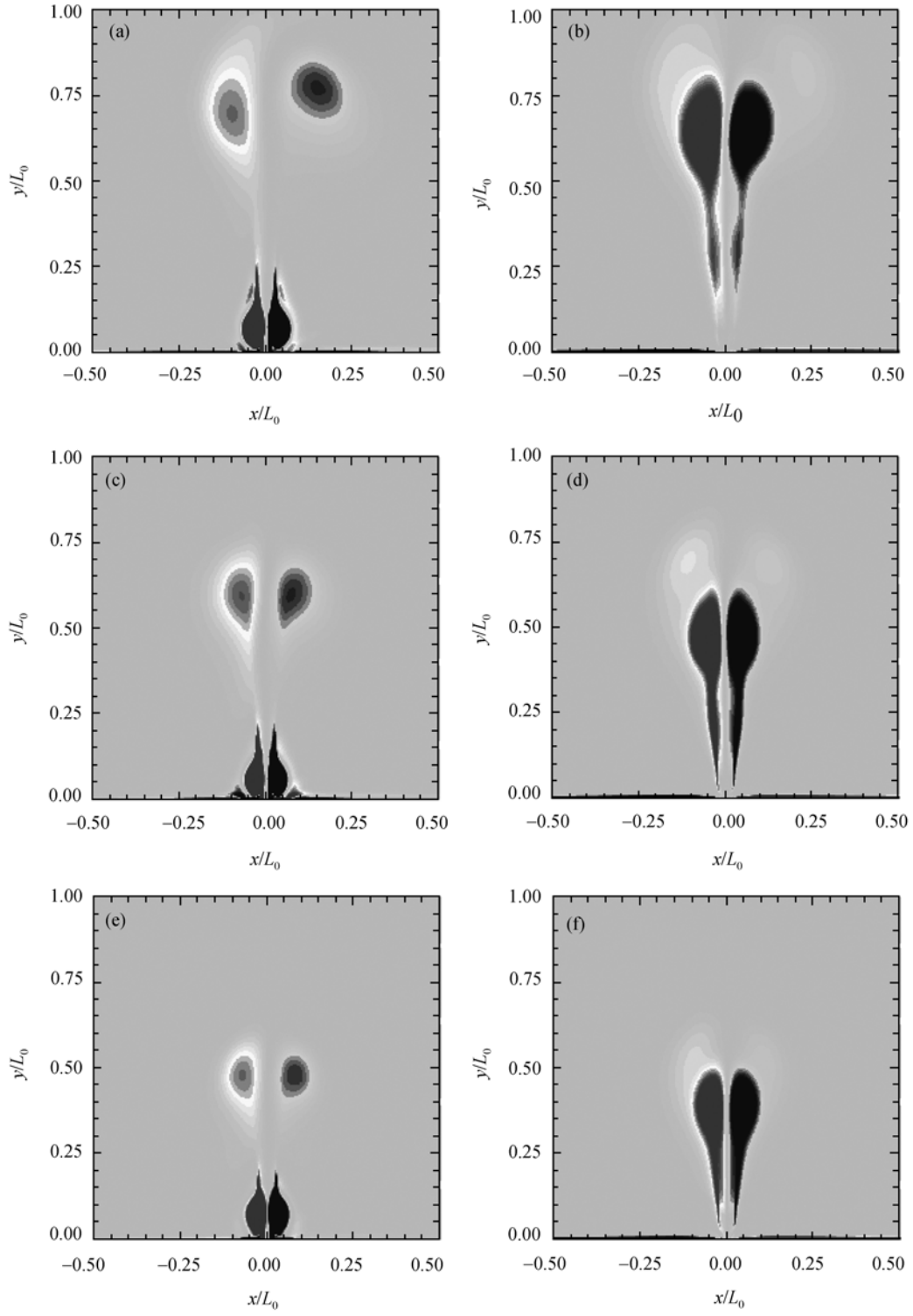

Figure 7 Evolution of the vortex pair of ZNMF jet during blowing and suction strokes[7]. (a) k=2, t/T=1/6; (b) k=2, t/T=2/3; (c) k=1, t/T=1/4; (d) k=1, t/T=3/4; (e) k=0.5, t/T=1/3; (f) k=0.5, t/T=5/6.

Reynolds number of the ZNMF jet increases with k, and the suction effect of the actuator on the vortex pair during the suction stroke decreases with the increase of k. So the vortex pair with a larger k value can have larger strength during the suction stroke and propagate further to form a larger scale jet in the far flow field.

Figure 8 shows the trajectories and the time averaged stream-wise velocities along the centerline with three different suction duty cycle factors k. It can be seen that the distance of the vortex pair and the time averaged stream-wise velocity increase with k, which is because that the strength of the vortex pair increases with k, and the self induced velocity also increases. The numerical simulation by Zhang and Wang[7] showed that the ZNMF jet with a different suction duty cycle factor k has similar characteristics to that actuated with traditional sine wave in previous studies.

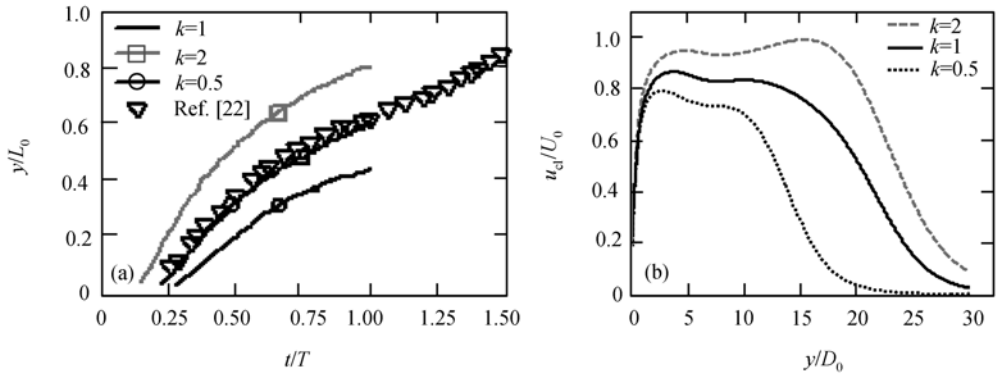

Figure 8 Effect of the suction duty factor k on the development of vortex pair[7]. (a) The trajectory of the vortex pair; (b) the time averaged stream wise velocity along the centerline of the actuator orifice.

2.2 Characteristics of ZNMF jet

The strength and the position of the vortex pair or ring are determined by the Reynolds number and the stroke length ratio when the vortex coalesces to synthesize a jet with momentum transfer to the embedding flow, but there still exist some uncharged characteristics for the formation of the ZNMF jet. The instant stream-wise velocities u_{cl}/U_0 at different stations along the centerline are presented in Figure 9. The curves of the instant stream-wise velocity in one period at the stations close to the orifice are similar to that of the sine wave, which represent the vibration of the membrane of the actuator. When the sample station is far from the orifice, the self induced velocity of the vortex pair or ring increases, and the suction effect of the actuator cavity on the vortex pair or ring during the suction stroke decreases, so the positive part of the instant velocity enhances and the negative part diminishes. At x/L_0=0.3, the peak suction velocity induced by the suction of the orifice goes to zero, which indicates that the entrainment of the orifice to the ambient fluid at this station during the suction stroke is insignificant and the vortex pair has been fully formed. After that, there

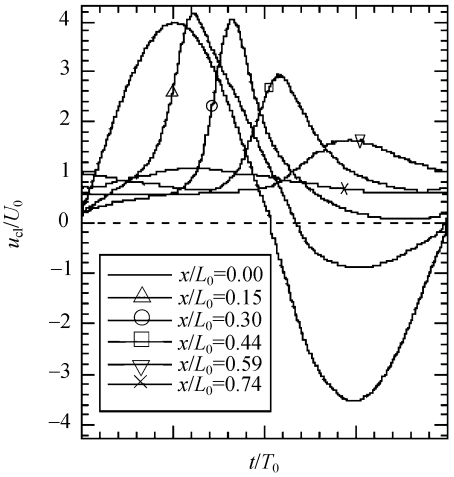

Figure 9 The variation of the instant stream-wise normalized velocities u_{cl}/U_0 in a period at different stations along the centerline, L=13.5, Re_{U_0}=695[28].

are more quiescent fluids entrained into the ZNMF jet with the development of the vortex pair or ring, which results in the decrease of the maximum velocity to satisfy the law of momentum conservation. These features of the stream-wise velocity variation along the centerline are independent of the two key parameters.

With the development of the vortex pair or ring of the ZNMF jet, the scale of the vortex pair or ring increases with the increase of its distance from the orifice. But the time averaged stream-wise velocity U decreases, which is caused by the more quiescent fluids entrained into the ZNMF jet (as shown in Figure 10(a)). If the velocity U is normalized by the time averaged velocity along the centerline U_{cl}, and the cross stream coordinate is normalized by the half local jet width b based on 0.5 U_{cl}, the cross stream distributions of the non-dimensional stream-wise velocity of the ZNMF jet collapse reasonably well, and they match well with the hyperbolic cosine function (as shown in Figure 10(b))[28]:

$$U / U_{cl} = \cosh^{-2}(\eta x / b),$$

where η is a parameter of the fit. Smith and Glezer[22,30], James and Jocobs[31], and Zhang and Wang[7] have the same conclusion by experiments or numerical simulations. This indicates that the stream-wise velocity distribution along the span-wise direction of the ZNMF jet has the same curve shape with that of the continuous jet. Smith and Glezer[22] indicated in their early study that the jet width b in the cross stream plane increases like $y^{0.88}$, but $b \propto y$ for conventional 2D jet. In a recent study on the comparison of ZNMF jet and conventional continuous jet, Smith and Swift[28] argued that the cross stream width b increases linearly with y, which is reasonably coincident with experimental results of Gordon et al.[32] and the numerical simulation result of Zhang and Wang[7].

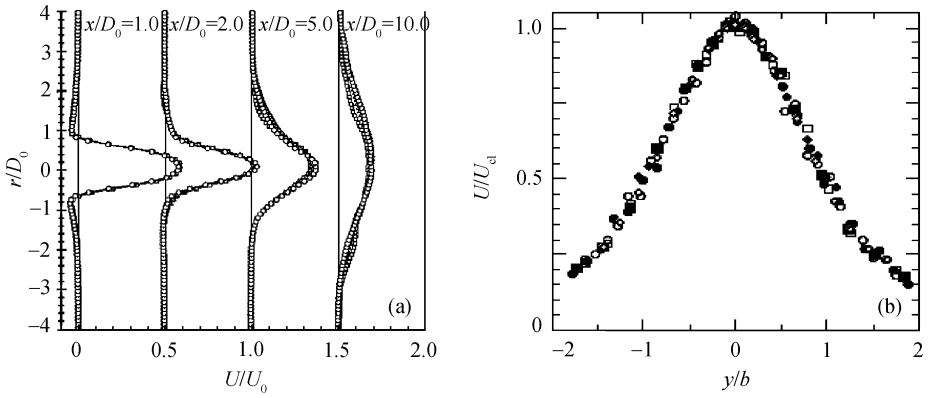

Figure 10 The time averaged stream-wise velocity distributions. (a) The velocity distributions at different stream-wise positions with L=2.0 and Re_{U_0}=2500, 5000, 10000[27]; (b) the normalized velocity distributions with L=17.0−80.8 and Re_{U_0}=734−2200, including that of the continuous jet[28].

3 Interaction of ZNMF jet with cross flow

Compared with the research about the development of the ZNMF jet in the quiescent flow, the development of the ZNMF jet in the cross flow and the flow structures produced by the ZNMF jet in the cross flow attracted less interests. In the research on the flow control by the ZNMF jet [33−36], it was found that the flow structure characteristics of the ZNMF jet interacted with the cross flow are very important for the control of the external or internal flow. In order to improve the ZNMF jet flow control efficiency, it is essential to study the interaction of the ZNMF jet with the cross flow

and to understand the mechanism for the ZNMF jet flow control method.

3.1 Flow structure of ZNMF jet interacted with cross flow

During the vortex ring formation of the circular ZNMF jet in the cross flow, the upstream branch of the vortex ring is significantly suppressed by the resident vorticity in the boundary layer, whereas the vorticity in the downstream part of the ring becomes intensified, because the vorticity in the downstream part and the boundary layer has the same sign. The asymmetric vortex ring undergoes subsequent tilting and stretching as it migrates across the boundary layer and propagates downstream[24]. Figure 11 shows the vortex structure of the circular ZNMF jet interacted with the cross flow by dye injection flow visualization in water tunnel. It is obvious that the upstream part of the vortex ring formed near the actuator orifice was weakened by the resident vorticity in the boundary layer, and the hairpin vortex structure formed by the interaction of the circular ZNMF jet with the cross flow, in which the hairpin vortex lifted up but the vortex legs connected the vortex head and the actuator orifice. NASA Langley research center investigated the trajectories of the circular ZNMF jet in the cross flow using PIV, LDV and hotwire measurements, and they also found that the hairpin vortex structure of the ZNMF jet interacted with the cross flow[37]. Many numerical simulation works[38−40] studied the hairpin vortex structure of the ZNMF jet in cross flow, and concluded that with the inducement of the hairpin the high speed fluid out of the boundary layer was injected into the low speed region in the boundary layer, and the relative low speed fluids were lifted up into the external flow. So the momentum of the boundary layer is enhanced and it can help the flow to overcome the adverse pressure gradient and to delay the boundary separation.

Figure 11 The flow structures produced by the circular ZNMF jet in cross flow, the actuator orifice is at the top of the image, and the flow direction is from right to left[24].

The ZNMF jet adds energy to the boundary layer in two different ways during the blowing and suction strokes. In the suction stroke of the actuator, since the ambient flow around the actuator has positive velocity component in the stream-wise direction, most of fluids which are sucked into the actuator cavity come from the upstream boundary layer of the actuator orifice (as shown in Figure 12(a)), which results in the thinner boundary layer and higher momentum of the upstream boundary layer. On the other hand, during the blowing stroke, the trajectory of the ZNMF jet tilts downstream induced by the cross flow (as shown in Figure 12(b)), and the hairpin vortex structure

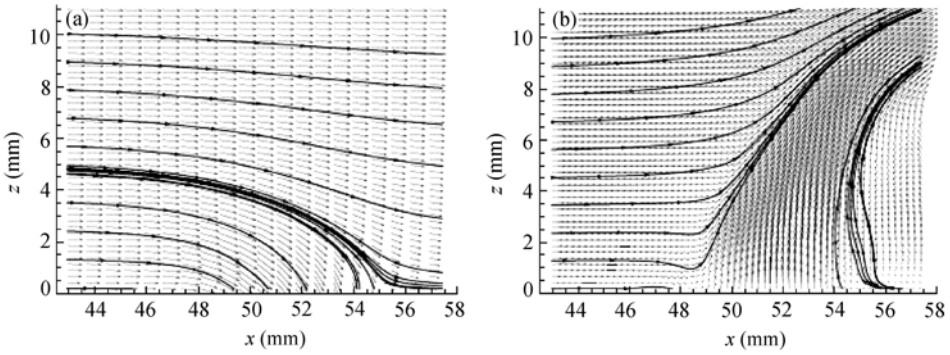

Figure 12 The velocity vector field and stream lines produced by the circular ZNMF jet in cross flow during suction and blowing strokes, the orifice is located at x=48−56 mm. (a) Suction; (b) blowing[41].

forms as discussed above, which results in the fluid with higher momentum to the downstream flow, almost tangentially to the control surface[41]. The average effective momentum added over the entire period replenishes the momentum deficit in the boundary layer. Therefore, the actuator not only produces momentum itself but also enhances the ability of the boundary layer to overcome adverse pressure gradients downstream through the mixing of the low momentum fluid near the surface with the high momentum external flow induced by the hairpin vortex structure. These flow structures promote boundary layer mixing and hence momentum exchange between the outer and inner parts of the boundary layer.

To investigate the time averaged flow field of the ZNMF jet in the cross flow, Gordon et al.[32] used the ensemble-averaged Planar Laser Induced Fluorescence (PLIF) images to get the trajectory of the ZNMF jet in the cross flow, which is identified by the maximum concentration of dye in the image. Two different flow patterns were observed in the images, which are henceforth classified as ‘‘single trajectory jets’’ and ‘‘jets with multiple trajectories’’ or ‘‘branches.’’ For the first pattern, the Strouhal numbers of the ZNMF jet are usually less than 0.02, and the jets maximum concentration is a single valued function of the cross-stream distance (as shown in Figure 13(a)). The trajectory of the jet is perpendicular to the wall up to 5*D*. As the distance from the wall increases, the trajectory bends in a downstream direction. The width of the jets is spread and the measured concentration of dye along the trajectory is reduced, because the scale of the vortex structure is enlarged and the strength reduced with more ambient fluids involved into the jets. The second pattern is occurred with St >0.02. It is characterized by two or more regions of high concentration issuing from the orifice per cycle (as shown in Figure 13(b)). Flow visualizations and the PIV measurements have confirmed that this pattern corresponds to a series of vortex rings formed by each pulse of the jet. In the ensemble average, a vortex ring traveling normal to the plane of the vortex core appears as two thin, high concentration regions separated by a region of low concentration at the locus of the ring center.

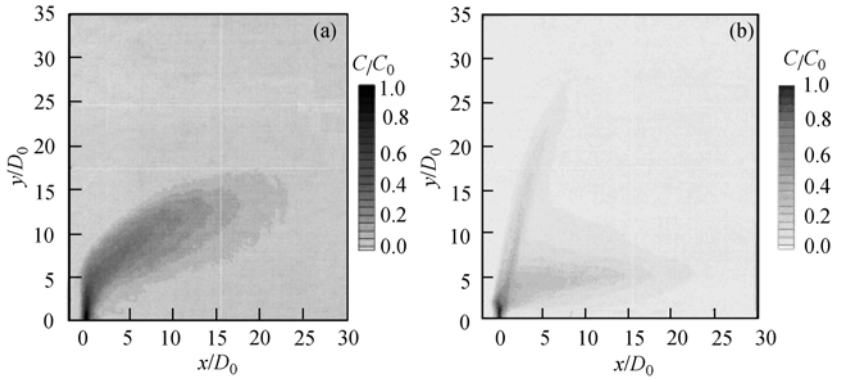

Figure 13 The trajectory of the vortex ring produced by the circular cylinder in cross flow obtained by ensemble-averaged Planar Laser Induced Fluorescence images[32]. (a) f=50 Hz, U_j = 7.10 m/s, St = 001, Re=14080, R=20; (b) f = 50 Hz, U_j=1.33 m/s, St = 0.077, Re=2640, R=10.

The primary flow parameter that has been identified in previous work about the ZNMF jet in cross flow is the ratio of jet momentum flux to cross flow momentum flux. This reduces to the ratio of velocities, $R=U_0/U_\infty$, which is known as the “velocity ratio” when the density of the jet flow fluid and the cross flow fluid are equal. Keffer and Baines1[42] found that the pressure effects could be neglected for high velocity ratios R>4, and that in this case the jet trajectory was only a function of

the velocity ratio. Pratte and Baines[43] used the power law relationship to fit the mean trajectory of the continuous jet in cross flow as follows:

$$\frac{y}{RD} = A\left(\frac{x}{RD}\right)^B,$$

where R is the velocity ratio, D is the scale of the orifice and A, B are the fit constants. To approximate the jet trajectories, the constants A and B in the equation can be varied to obtain a curve of best fit. Gordon et al.[32] used this equation to fit the trajectory of the ZNMF jet in cross flow with the velocity ratios R=4.6 and 7.0, which were estimated with the maximum concentration of dye and the maximum velocity points. The region for the constant variation is consistent with that of the continuous jet in cross flow (listed in Table 1), which indicates that the trajectory of the ZNMF jet in cross flow is similar to that of the continuous jet.

Table 1 The fit constants in analysis formula of the ZNMF jet and continuous jet

Literature		Constant A	Constant B
Smith and Mungal[44], continuous jet, dye concentration		1.5	0.27
Pratte and Baines[43], continuous jet, dye concentration		2.05	0.28
Hasselbrink and Mungal[45], continuous jet, analysis model		-	0.33
Gordon et al.[32], ZNMF jet, R=4.6	dye concentration	2.08	0.28
	maximum velocity	2.16	0.27
Gordon et al.[32], ZNMF jet, R=7.0	dye concentration	1.51	0.37
	maximum velocity	1.74	0.34

Ugrina[46] measured the instant velocity of the ZNMF jet interacted with the cross flow by hotwire. The contours of time averaged velocity in the plane along the centerline of the orifice are presented in Figure 14(b), in which the curves with the maximum velocity points are corresponding to the trajectory of the vortex ring of the ZNMF jet in cross flow. He also built up a simplified model offering the ability to investigate the sensitivity of the character of the flow field produced by ZNMF jet in cross flow to jet velocity, location and jet diameter. A control volume concept and integral techniques were used to monitor the global quantities along the jet centerline. The model required assumptions to be made about the jet cross sectional shape, entrainment rate and surface

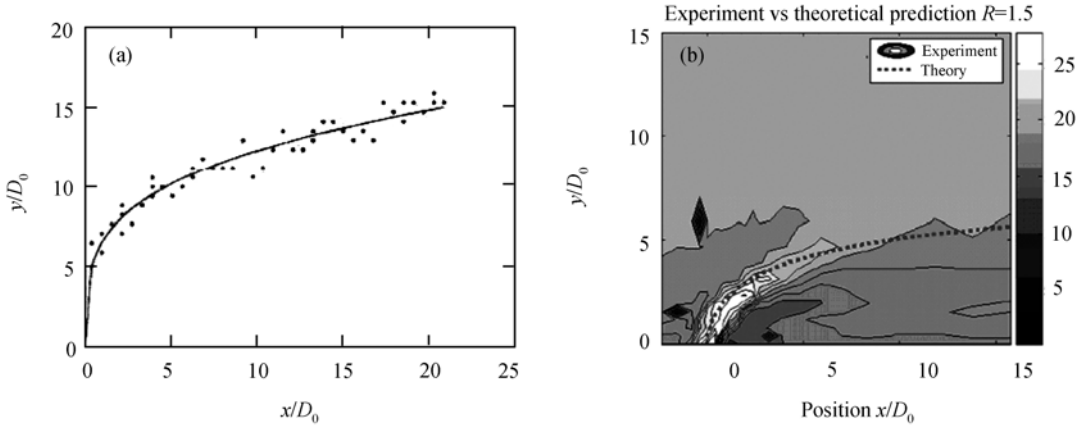

Figure 14 The trajectories of the ZNMF jet in cross flow. (a) R=4.6, A=2.16, B=0.27, the scatted points obtained by estimating the maximum velocity, the curve is the fitted by analysis model[32]; (b) the contours of velocity at R=1.5, the dashed line is predicted by analysis model[46].

forces coefficients. The trajectory of the vortex ring of the ZNMF jet in cross flow predicted by the analysis model is also presented in Figure 14(b), which matches well with that estimated by the experimental data obtained with hotwire. It can be seen that the trajectory predicted by the analysis model and hotwire measurement in Figure 14(b) is much similar to that obtained by Gordon et al.[32] with PIV measurement in Figure 14(a), which indicates that the trajectory of the vortex pair or ring of the ZNMF jet in cross flow can be well predicted.

3.2 Effect of key parameters on flow field produced by ZNMF jet in cross flow

According to the dimensional analysis in section 2.1, the development of ZNMF jet in cross flow is affected not only by the two key parameters about the actuator described above but also by the key parameters associated with the cross flow. Since the working fluid of the actuator is the same as that of the cross flow, the additional key parameters associated with the cross flow are the incoming flow velocity U_∞ and the boundary layer thickness δ at the location of the actuator. The corresponding non-dimensional parameters normalized by the time-averaged blowing velocity U_0 and the scale of the orifice D_0 are the velocity ratio $R=U_0/U_\infty$ and the boundary layer thickness to the scale of the orifice ratio δ/D_0, respectively.

Ugrina[46] studied various velocity ratio cases to find the threshold that would allow the ZNMF jet to penetrate boundary layers, and found that the critical velocity ratio was 1.0 when this occurred in the flow field topologies studied. With $R<1.0$, depending on the self induced velocity and strength of the vortex ring, it was expected that the ZNMF jet would block the boundary layer, causing the cross flow to be diverted over. However, at low velocity ratios, the cross flow exerts sufficient pressure on the orifice, and there is no strong vertical jet momentum visible. It seems that the jet is quickly deflected, losing its structure to the dominating influence of the external cross flow. The influence of the ZNMF jet remains completely buried inside the boundary layer, just barely perturbing and shuffling the near-wall flow. The ZNMF jet is swept along with the cross flow, introducing turbulence to the flow and inducing just a slight lift up of the oncoming flow immediately above and slightly downstream from the orifice, effectively causing a minor thickening of the boundary layer. As the velocity ratio increases, the ZNMF jet ability to push the boundary layer away from the wall also increases. So the amount of displacement of these streamlines could arguably be used as a measure of control authority of the actuator as the velocity ratio is less than 1.0. With higher velocity ratios $R>1.0$, the ZNMF jet is stronger and can shift the external flow momentum. The ZNMF jet perforates much deeper into the cross flow and well beyond the edge of the boundary layer. The forming of a vortex ring appears to block the boundary layer flow entirely, slowing it down, causing the external streamlines to partially divert around and to partially be entrained in the forming vortex rings. As the velocity ratio increases, the ZNMF jet becomes stronger, and the slope of the ZNMF jet trajectory also increases. At a velocity ratio of 6, the ZNMF jet was standing in the cross flow almost entirely vertically. In all cases, a region of separated, low pressure flow was created downstream of the jet orifice. So the local pressure distribution on the wall was changed as a result of the actuator effect.

Mittal and Rampunggoon[47] investigated the interaction of the 2D slot ZNMF jet with the flat plate boundary layer by numerical simulation. At the velocity ratio $R=0.3$, it was observed that the counterclockwise vorticity was cancelled quickly. Furthermore, the clockwise vortices were found not to penetrate to the free stream side of the boundary layer. Consequently, there was no high momentum external flow entrained. As the velocity ratio increased to 0.67, the counterclockwise

rotating vortex was cancelled out by the boundary layer, which was composed of clockwise vorticity. In contrast, the clockwise vortex entrains fluid from the boundary layer and from the external flow and grew in size as it convected downstream. The entrainment of high momentum external fluid into the boundary layer by this clockwise vortex is an important feature since it has been hypothesized that this makes the resulting boundary layer more resistant to separation. With R=3.0, the vortex pair formed during the blowing stroke immediately comes out of the flat plate boundary layer and begins to convect downstream. The velocity ratio threshold R=0.67 in this article for the ZNMF jet to penetrate boundary layers is different from that obtained by Ugrina[46]. This is because the orifice here in numerical simulation is a 2D slot, but in Ugrina's experiment it was a 3D circular hole. Otherwise, the difference of the incoming flow, for example the boundary layer thickness, will also contribute to the divergence. Mittal and Rampunggoon[48] found that the ZNMF jet had the ability to form a large mean recirculation zone in the cross flow by numerical simulation (as shown in Figure 15(a)). It has been suggested that this so-called virtual aero-shaping effect is one mechanism through which the ZNMF jet modifies the shape of the lift body, consequently alters the pressure gradient and improves the lift efficiency. Figure 15(b) presents the relationship between the length of the recirculation zone induced by the ZNMF jet in cross flow and the momentum coefficient of the jet, and it can be seen that the normalized bubble length grows linearly with the momentum coefficient. A least-square linear fit has also been performed for the entire data and the slope of the line is determined to be 1.03.

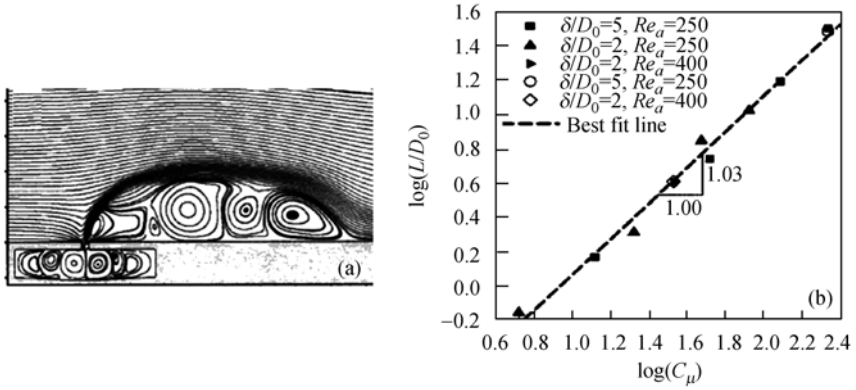

Figure 15 The recirculation region induced by the ZNMF jet in cross flow[48]. (a) δ/D_0 =5, R=5; (b) the length of the recirculation region vs. the jet momentum coefficient.

Zhong et al.[24] studied the effect of the velocity ratio and the stroke length ratio on the flow structures produced by the ZNMF jet in the cross flow with dye injection flow visualization in a water tunnel. With the velocity ratio increase, three vortex structures were observed in the experiments, which are the hairpin vortex, the stretched vortex ring and the turbulent vortex ring (as shown in Figure 16(a)). They also concluded that the velocity ratio determines the steepness of the trajectory of the structures as they propagate downstream, which is consistent with that obtained by Ugrina[46]. They argued that the Strouhal number St defined using the freestream velocity mainly affects the spacing between consecutive structures. A graph illustrating the range of velocity ratio, Strouhal number and stroke length where three types of structures are produced is presented in Figure 16(b). It can be seen that within the range of Strouhal number tested in their experiments, the range of velocity ratio and stroke length within which hairpin vortices and stretched vortex

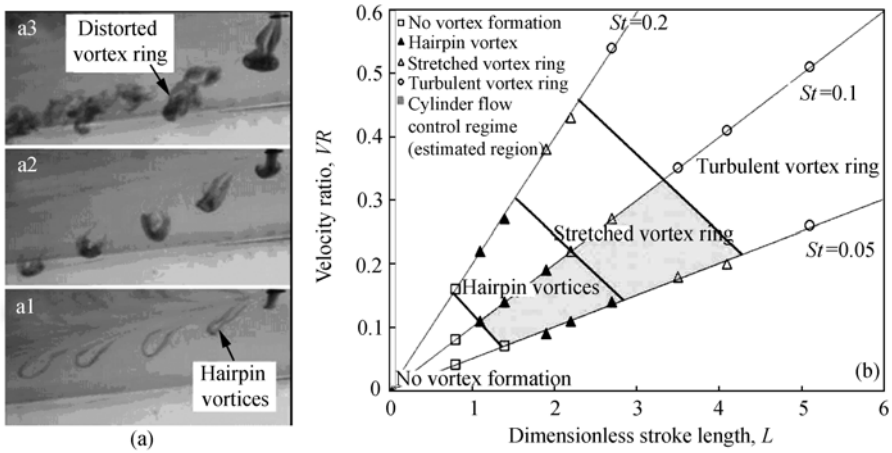

Figure 16 The flow structures produced by the ZNMF jet in cross flow visualized by dye injection with different parameters [24]. (a) Three typical vortex structures; (b) the effect of velocity ratio and stroke length ratio on the flow structure.

rings are expected to be seen are approximately from 0.1 to 0.5 and from 1.0 to 5.0, respectively. According to the conclusion of Crook and Wood[49] drawn from the experiments, these two flow structures produced by the ZNMF jet can control the boundary layer separation on the circular cylinder efficiently.

The scale of the orifice to the thickness of the boundary layer δ/D_0 is an interesting non-dimensional factor that influences the global flow field topology of the ZNMF jet in cross flow. The importance of this parameter on flows has barely been studied in the literature, although some researchers mentioned this issue in their works[32,47]. Ugrina[46] investigated the effect of the orifice scale on the thickness of the boundary layer ratio δ/D_0 on the flow structures produced by the ZNMF jet in cross flow by varying the diameters of the orifice. In order to keep the velocity ratio and the momentum coefficient of the ZNMF jet as constants, the actuator frequency should be increased with the increase of the orifice diameter. Consequently, the scale of the vortex structure induced by the ZNMF jet grew, and the distance of the vortex structure from the orifice decreased, which resulted from the decrease of the stroke length ratio. They concluded that thinner boundary layers implied a flow with more momentum, which imposes a stronger impact on the oncoming jet causing it to deflect earlier. Actually, the boundary layer thickness has a close relationship with the incoming flow velocity. In order to keep the actuator parameters as constants, the incoming flow velocity profile should be modified to study the effect of the scale of the orifice on the thickness of the boundary layer δ/D_0, which can be realized by advancing the boundary layer transition or placing the ZNMF jet actuator at different stream-wise positions along the flat plate.

4 Applications of ZNMF jet in separation control

Because the ZNMF jet has the unique feature discussed previously, it has become a popular active flow control method since it was first used as a flow control method in the laboratory in 1990's. The present review mainly introduces the state of art of the ZNMF jet used as a separation flow control method and its application in improving the aerodynamic characteristics of air vehicles. The other applications of the ZNMF jet, such as jet vectoring, fuel mixing, enhancing heat transfer, suppressing the noise, etc., can be seen in ref. [4].

4.1 Boundary layer separation control of circular cylinder

The ZNMF jet was first used as a separation control method to control the boundary layer separation of the circular cylinder by Amitay et al.[50]. The center section of the cylinder model is instrumented with a pair of adjacent rectangular ZNMF jet actuators that are spaced 2.5 mm apart along the long side of their orifices. The azimuthal jet location relative to the front stagnation point γ is varied by rotating the cylinder around its axis. Figure 17 presents the smoke flow visualization images in the wind tunnel of the flow structures around the circular cylinder controlled by the ZNMF jet with different parameters. When the jets are placed at γ=60º (Figure 17(b)), and are operated in phase with the combined $C_\mu \sim O(10^{-3})$, it is apparent that the separation point on the top surface moves downstream and the front stagnation point is displaced below the x axis. When the jets are placed at γ=180º and C_μ is increased to $O(10^{-1})$ (Figure 17(c)), the external flow appears to be almost attached to the surface of the cylinder. Finally, in Figure 17(d) the jets are still placed at γ=180º but they are operated out of phase such that the bottom jet is leading by $2\pi/3$. The vectoring of the jets results in downward deflection of the entire wake and a concomitant displacement of the front stagnation point, which is qualitatively similar to classical flow visualization snapshots of the flow around a spinning cylinder. The decrease and increase in the spacing between streak lines above and below the cylinder, respectively are indicative of a change in circulation and generation of lift. Meanwhile, Amitay et al.[50] presented the velocity deficit and the turbulent stresses across the entire wake corresponding to Figure 17(b). They are all substantially reduced, which may be attributed to the reduction in the scale of the shed vortices and enhanced dissipation.

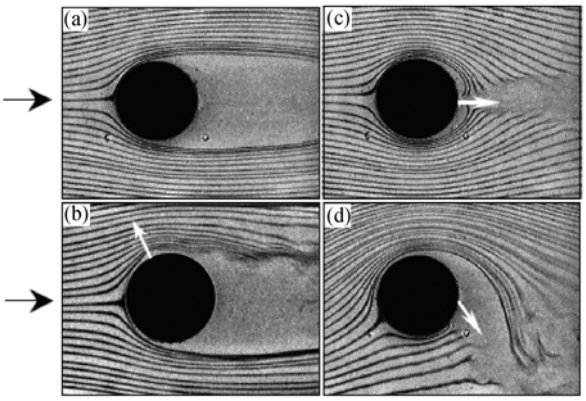

Figure 17 The effect of the ZNMF jet on the separation flow control of the circular cylinder visualized by smoke wire. (a) No control; (b) azimuthal angle γ=60º, (c) γ=180º, (d) γ=180º, jet angle with respect to the wall Φ=120º[50].

Amitay el al.[50] concluded that the interaction of the ZNMF jet with the embedding flow leads to the formation of closed recirculation regions and thus to an apparent modification of the flow boundary layer on scales that are one to two orders of magnitude larger than the characteristic length scale of the jets themselves, which is so called the visual aero-shaping effect, so the flow structure around the circular cylinder has been dramatically changed. Honohan et al.[51] measured the velocity field around the circular cylinder controlled by the ZNMF jet actuator by PIV. The quasi-steady recirculation zone was found close to the location of the actuator orifice, as the actuator dimensionless frequency was one order of magnitude higher than the characteristic frequency of the unforced flow, which resulted in the substantial thinner boundary layer and a favorable stream-wise pressure gradient downstream of the actuator. So the boundary layer separation point on the circular cylinder can be delayed.

The response-surface method in combination with an LES/DNS numerical approach has been applied to finding the minimum drag coefficient of the circular cylinder subject to control via ZNMF jet by Catalanoy et al.[52]. Their work has been performed using the location and the fre-

quency as parameters to optimize, while keeping the amplitude fixed with a momentum coefficient of 6.5×10^{-3}. The optimum locations for the actuator were near the boundary separation point and the optimum actuating frequencies were 4.4 and 9.21 times of the natural shedding frequency of the flow for *Re*=500 and 3900, respectively. A decrease of about 4% in drag has been achieved at *Re*=500, and the drag reduction at *Re*=3900 was about 13% according to 2D computations, but this result was not reproduced in 3D with the same set of control parameters at *Re*=3900.

Circular cylinder separation control and flow structure influenced by the ZNMF jet have been experimentally investigated in a water tunnel by Wang et al.[8]. The actuator orifice of the 2D slot ZNMF jet was toward upstream from the front stagnation point of the cylinder. When Reynolds number based on the ZNMF jet average exit orifice velocity is lower than 43, the cylinder front stagnation point moves upstream and a closed envelope forms in front of the windward side of the cylinder during the blowing stroke of the ZNMF jet, which acts as an apparent modification for the cylinder configuration. Figures 18(a) and 18(b) show the flow field around the circular cylinder controlled by the ZNMF jet obtained by the hydrogen bubble flow visualization and the PIV measurement, and the flow topology is shown in Figure 18(c). The separation region behind the cylinder is reduced during both blowing and suction strokes, but there still exists wake vortex shedding which is the vortex structure induced by the ZNMF jet near the leading edge of the cylinder with their shedding frequency identical to the actuator frequency, and the lock-in phenomenon appears. The vortex pair induced by the actuator at the stagnation point shedding from the circular cylinder is presented in Figure 18(d).

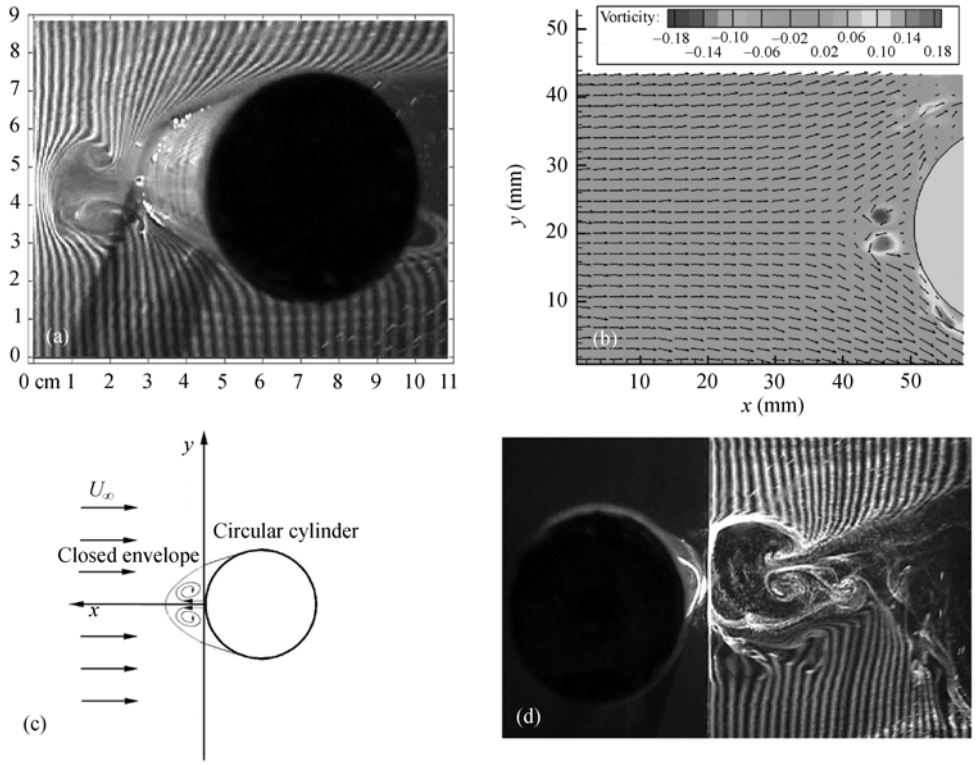

Figure 18 The flow structure close to the stagnation point and in the wake of the circular cylinder with closed envelope formed, *L*=99.5, *f* =0.5 Hz, Re_{U_0}=43. (a) Flow structure in the stagnation region; (b) velocity vector and vorticity field in the stagnation region; (c) topology structure of the closed envelope flow pattern; (d) flow structure in the wake[8].

For high Reynolds case, the region influenced by the ZNMF jet along stream-wise and vertical direction is gradually enlarged, and an open envelope forms upstream of the cylinder as shown in Figurs 19(a) and 19(b). When Reynolds number is greater than 344, the separation region disappears and the flow around the cylinder is fully attached. A new vortex pair shedding periodically is generated near the back stagnation point of the circular cylinder. Figures 19(c) and 19(d) show the flow field obtained by the hydrogen bubble flow visualization and the PIV measurement, respectively.

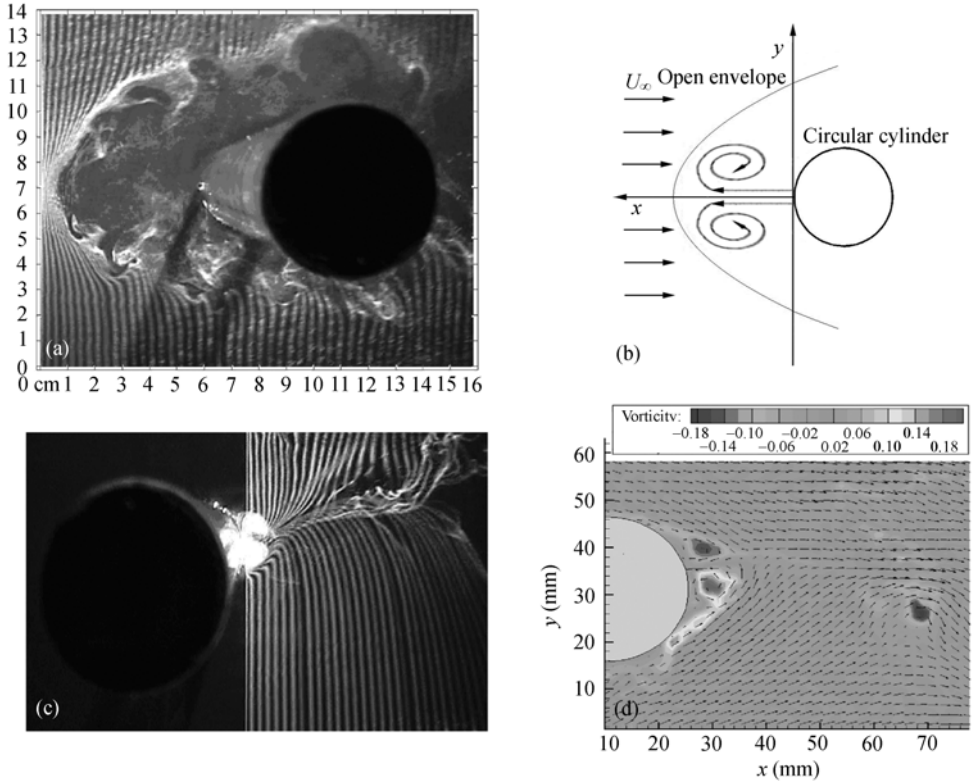

Figure 19 The flow structure close to the stagnation point and in the wake of the circular cylinder with open envelope formed. (a) Flow structure in the stagnation region, L=27.1, f=4 Hz, Re_{U_0}=94; (b) topology structure of open envelope flow pattern; (c) flow structure in the wake, L = 99.5, f = 9 Hz, Re_{U_0} = 774; (d) velocity vector and vorticity field in the stagnation region, L = 99.5, f = 9 Hz, Re_{U_0} = 774[8].

Based on the numerical simulation by Zhang and Wang[7], Feng et al.[9] used the novel signal wave pattern to generate high efficient ZNMF jet for the circular cylinder separation control by experiments. The actuator orifice was toward the down stream of the cylinder in their study. Figure 20 shows the effect of suction duty factor k on the boundary layer separation control of the circular cylinder at the exciting frequency f=4 Hz. As k=1.0, there is also a narrow separation region existing downstream of the circular cylinder. When the suction duty factor k decreases to 0.25, the separation region downstream of the cylinder becomes larger, which means the efficiency of the ZNMF jet on separation control is reduced. As the suction duty factor k increases to 2.3, there is no much difference for the separation region compared with that at k=1, but with k increasing high enough, the exit orifice velocity and vortex strength increase greatly and the efficiency of the ZNMF jet on separation control is significantly improved, which validates the novel signal wave pattern for high efficient ZNMF jet generation.

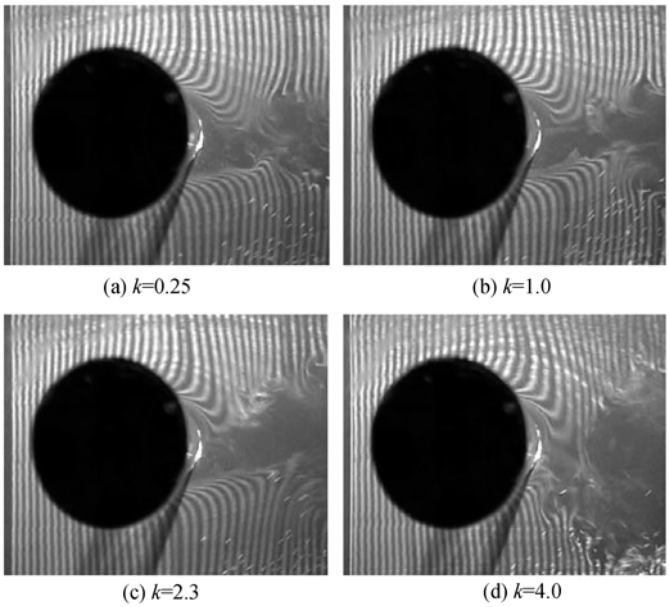

Figure 20 The effect of suction duty factor k on the flow separation control around the circular cylinder (L=99.5, f=4 Hz).

4.2 Flow separation control around airfoil and parameter optimization

Smith et al.[53], Amitay and Glezer[54,55] used the ZNMF jet actuators for the suppression of separation over an unconventional airfoil, which is composed of an aluminum leading edge circular cylinder mounted within a fiberglass aerodynamic fairing that is based on an uniformly stretched NACA0015 symmetric airfoil. The center section of the cylinder houses a pair of adjacent synthetic jet actuators and can be rotated about its axis within the fairing, so the location of the actuator can be adjusted relative to the airfoil. When the actuators are typically operated at dimensionless frequencies that are one order of magnitude higher than the shedding frequency of the airfoil (St =O(10), based on the airfoil chord length and the incoming flow velocity), the boundary layer separation point on the suction side of the airfoil can be delayed, which results in the improvement of the airfoil aerodynamic characteristics. Smith et al.[53] found that the stall attack angle of the airfoil could be delayed from 5º to 18º, and the lift to drag ratio also could be increased. Amitay and Glezer[54,55] studied the effect of the exciting frequency of the ZNMF jet actuator on the flow separation control around the airfoil. The flow structure was obtained by the flow visualization technique, and the velocity deficit in the wake was measured by hotwire. They concluded that the lift to pressure drag ratio L/D_p has different trends at two ranges of jet actuation frequencies St. As St <4, the lift to pressure drag ratio L/D_p decreases with the increase of the exciting frequency. As St >10, the lift to pressure drag ratio L/D_p increases by 27% compared with that of the unforced case and has little difference with

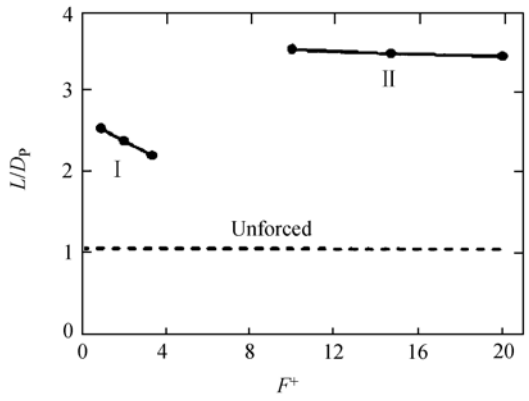

Figure 21 The variation of the lift to pressure drag of the airfoil with respect to the reduced actuator frequency[54].

the exciting frequency variation (see Figure 21). When the attack angle of the airfoil is 20º, the angle between the jets' centerline and the free stream is 45º, the momentum coefficient is 4.5×10^{-3} and the actuator frequency is at the order of $O(1)$, the interaction of the ZNMF jet with the separation boundary layer results in a series of small vortices and the large separation region diminishes. With the increase of the actuator frequency, the scale of the vortices decreases. When the actuator frequency increases to the order of $O(10)$, the small scale vortices around the actuator orifice disappears and the separated shear layer fully attaches to the airfoil.

The different aerodynamic characteristics between the airfoils forced by the high frequency actuator and the low frequency one can be attributed to the different excitation mechanisms. At low frequency, the separation shear layer attaches to the airfoil in the time averaged flow field, but the instant flow field contains a lot of small vortices produced by the ZNMF jet. The lift of airfoil will increase under the control of the ZNMF jet, so does the fluctuation of the lift and drag. Zhang and wang[56] also presented the small vortices induced by the interaction of the ZNMF jet with the separated shear layer on the suction side of the airfoil, which results in the small recirculation region and the enhancement of the lift (as shown in Figure 22). But with high frequency, a quasi steady recirculation region will appear, and the local aerodynamic shape of the lift body is modified. So the boundary layer thickness and the pressure distribution are changed, which results in the aerodynamic characteristics improvement of the lift body. The quasi steady recirculation region induced by high frequency actuator is also confirmed by Honohan et al.[51] with experiments and by Mittal and Rampunggoon[47,48] with numerical simulations.

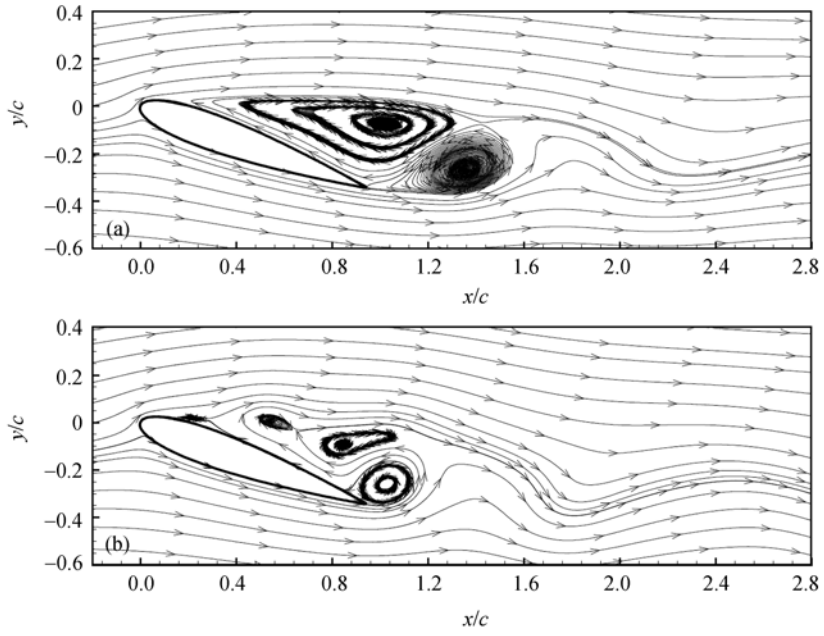

Figure 22 The flow structures around the NACA0015 airfoil with/without ZNMF jet control. (a) Without control; (b) with control[56].

Duvigneau and Visonneau[34] simulated and optimized a ZNMF jet actuator for aerodynamic stall control of the flow around the NACA 0015 airfoil by solving unsteady Reynolds-averaged Navier-Stokes equations. The flow control parameters adopted in Gilarranz's experiments[57] were considered as starting point for the optimization, in which the velocity ratio was 1.37, the dimen-

sionless actuator frequency was 1.29 and the jet was perpendicular to the wall of the airfoil. The objective function in their study was the time-averaged lift coefficient. An increase of 52% of the maximum lift coefficient with respect to the baseline airfoil was achieved in the attack angle range of 16º—22º. Meanwhile, the drag of the airfoil with the ZNMF jet flow control decreased a lot after stall angle, so the lift to drag ratio could be greatly enhanced.

The optimum velocity ratio of the ZNMF jet was 1.72 in the simulation and optimization of Duvigneau and Visonneau[34]. Seifert[58] and Ravindran[59] concluded that the lift of the airfoil controlled by tangential blowing ZNMF jet increased with the momentum coefficient in the experiments and numerical simulation, respectively. Zhang and Wang[56] studied the aerodynamic characteristics of a NACA0015 airfoil forced by an actuator located at 13% chord length of the airfoil, and indicated that the efficiency of the ZNMF jet increased with the increase of velocity ratio, which means the lift of the airfoil increases monotonously with the momentum coefficient. Tuck and Soria[60] controlled the flow around a NACA0015 airfoil with the actuator located at the front stagnation point of the airfoil, and the jet was opposite to the incoming flow. When the actuator dimensionless frequency was 1.3, the lift coefficient of the airfoil increased monotonously with the momentum coefficient. However, when the actuator dimensionless frequency was 0.6, there existed an optimum momentum coefficient at C_μ=0.14%, after that the increase of momentum coefficient would result in the decrease of lift of the airfoil. For the jet angle with respect to the wall, the optimum value obtained by Duvigneau and Visonneau[34] was 25º, which was consistent with that of Seifert[58] in experiments and Ravindran[59] and Donovan el al.[61] in numerical simulation. Zhang and Wang[56] analyzed the mechanism of the flow separation control around the airfoil by low frequency ZNMF jet actuator with numerical simulation. They pointed out that, in the suction stroke, the low momentum fluid in the boundary layer upstream of the orifice was sucked into the cavity, so the boundary layer thickness was reduced, and the energy of the boundary layer increased. During the blowing stroke, the ZNMF jet tilts to the downstream suppressed by the external flow, and the clockwise vortex is enhanced. With the inducement of the clockwise vortex, the mixing between the high momentum external flow and the low momentum boundary layer flow will be increased, which add the momentum to the boundary layer downstream of the orifice. In these two ways, the boundary layer has more energy to resist the adverse pressure gradient, and the separation point can be delayed. This conclusion agrees with that of Schaeffler[41], who presented the flow field produced by the ZNMF jet in cross flow during the blowing and suction strokes by numerical simulation. Milanovic and Zaman[62], Zhong et al.[63] investigated the effect of the jet angle with respect to the wall on the flow structures induced by the circular ZNMF jet in cross flow, and indicated that the time averaged blowing velocity over the orifice and the strength of the stream wise vortex would be enhanced with the jet angle at 45º with respect to the wall, with which the flow separation could be successfully controlled.

The optimum dimensionless frequency obtained by Duvigneau and Visonneau[34] is 0.85, except for the case at attack angle α=22º, which consists with the optimum dimensionless frequency about 1.0 in Seifert's experiment[58]. Seifert and Pack[64] argued that the optimum control could be achieved when there were four small scale vortices in the separation region, which resulted in the optimum dimensionless exciting frequency 1.0. Suzuki[65] studied the effects of an oscillatory ZNMF jet acting on the flow over a half-cylindrical hump in two dimensions. The DNS results have shown that periodic actuation breaks large-scale vortices that are generated in the natural case into smaller vortices and delays the separation point at the dimensionless frequency St=1, but they

found that there was no improvement for the aerodynamic performance when the actuator frequency was in the range of $St=O(10)$, which is the optimum frequency found by Amitay and Glezer[54,55] to control the separation of the flow around an unconventional airfoil. Suzuki[65] suggested that the reason is that the laminar flow simulations lack some features of a turbulent boundary layer, and the natural separation phenomenon is different for two- and three-dimensional bodies. Dandois et al.[66] performed numerical simulations of the controlled flow over a smooth ramp to study the influence of ZNMF jet frequency by solving the N-S equations with LES/DNS. For St=0.5, the separation length is reduced by half for a velocity ratio of 0.5. This frequency corresponds to the presence of a single large vortex in the separated zone and is close to the natural shedding frequency. But the effect of the high frequency forcing at St=4 is an increase of the separation length by 43 % (see Figure 23). Brunn and Nitsche[67] studied the effect of the ZNMF jet flow control on the wake of the Ahmed vehicle mode. Forcing frequencies in the range of the initial shear layer Kelvin-Helmholtz instability and the vortex-shedding were used to test the receptivity of the flow, which are St=0.1 and 0.3, respectively. They found that the velocity fluctuations in the shear layers increased at St=0.1, so the momentum transfer between the separation region and the outer flow also increased, resulting in a substantial reduction of the reattachment length and reduction of vehicle drag by 23%.

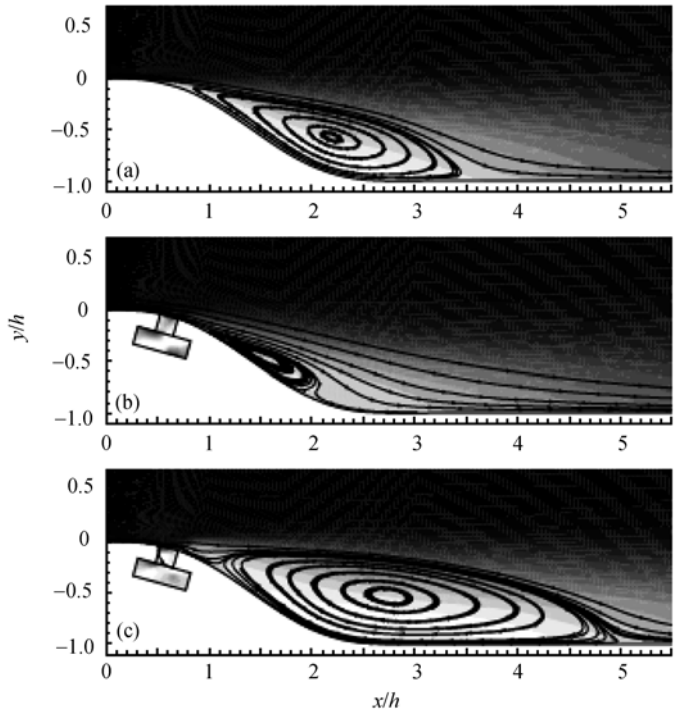

Figure 23 The time averaged recirculation region downstream of the hump actuated by ZNMF jet. (a) Without control; (b) St =0.5; (c) St =4[51].

Similar to the application of the ZNMF jet in flow separation control on the airfoil, the applications of ZNMF jet on flow separation control in turbo fan and diffuser are also widely investigated. But there is no uniform conclusion for the optimum parameters of the ZNMF jet, such as the location, the actuator frequency, the velocity ratio, and so on. Since the variation of these parameters will result in different transition and separation behavior, the flow separation mechanism

changes, followed by the optimum working parameters. The detailed investigation about the optimization of the actuator parameter for the separation control requires the systematic research on the interaction of the ZNMF jet with the cross flow and the ZNMF jet flow separation control in a larger range of parameters.

4.3 Application of ZNMF jet flow control on air vehicles

For the conventional air vehicles, the slot wing and flap wing are popularly used as the two effective passive flow control methods. In recent years, the new concept aerodynamic configurations, such as the blend wing body and the MAVs, have much higher requirement for the flow control method, so the active flow control method will inevitably be the substitute in the new century. What is more, the ZNMF jet actuator can be highly integrated by MEMS technique with the development of material science and manufactory technique. Figure 24 presents the newly invented micro ZNMF jet actuator by Parviz et al.[68] of Michigan University. The wafer contains about 1000 resonators configured in four individually addressable quadrants. The inset shows six resonators surrounding an ejector opening, and details of the non-uniform hole distribution on the actuator back-plate. The highest jet velocity measured was above 16 m/s, which is adequate for the flow control on the MAVs. It is essential that the ZNMF jet actuator fabricated with MEMS technology will be more attractive in flow control of both external and internal flows in the future.

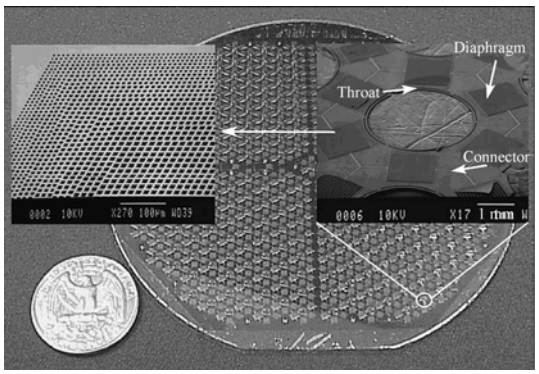

Figure 24 The wafer integrated with ZNMF jet actuators, next to a US quarter coin[68].

Experiments have been performed since 2000 by Georgia Institute of Technology to investigate the control of the flow field around the stator vanes of a new mini ducted fan unmanned aerial vehicle (UAV) BAGEL using ZNMF jet actuators. The sketch of the UAV is shown in Figure 25(a). The duct diameter is 11 inches and the depth is 5 inches. The aerodynamic force was produced by the three blades propeller, and the brushless DC electric motor was mounted in the duct with four stator vanes. The section of the stator is a Clark-Y airfoil, which has 10º attack angle with respect to the incoming flow in the duct. When the UAV is hovering, the flow around the stator blade will fully attached to the airfoil to result in the lift and the torsion to balance that produced by the rotor. If the UAV does a slow speed translating flight, the attack angle of the stator to the incoming flow increases, which results in the flow separation around the stator airfoil and the variation of the aerodynamic forces (see Figure 25(b)), so the moment equilibrium no longer exists. Fung and Amitay[69] studied the effect of the ZNMF jet actuator on the flow around the UAV stator vane, and they pursued to balance the moment of the BAGEL UAV by this active flow control method. Because the flow fully attaches to the Clark-Y airfoil in the static model experiments, which is different from that of the UAV in translating flight, Fung and Amitay[69] induced separation on the stator vane at a desired stream-wise location (21% c, here c is the airfoil length) by placing a small passive obstruction on the suction side of the stator vane, which is based on the work of Chatlynne et al.[71] and Amitay et al.[72] on a two-dimensional Clark-Y airfoil model. The ZNMF jet actuator was placed at corresponding dimensionless stream-wise location of x/c=0.25.

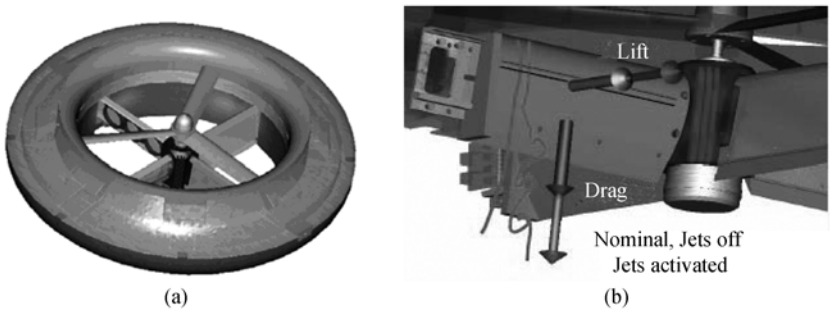

Figure 25 Application of the ZNMF jet separation flow control on the BAGEL mini duct fan MAV. (a) Configuration of the actuators on the MAV; (b) aerodynamic forces variation with control[69].

Figure 26 presents the detailed velocity vector fields above the stator vane at three radial locations r/R=0.26, 0.44, and 0.70 for the rotor speed 4300 r/min, in which the baseline cases are presented on the top, and the controlled ones are in bottom. In the sections at r/R=0.26, 0.44, the flow separated in the down stream of the obstruction for the baseline, and the suction surface of the airfoil in the picture view is in the adverse flow region. With the ZNMF jet flow control, the activation results in a closed recirculation region, and in the down stream of this region the flow is completely attached to the surface of the stator. In the section at r/R=0.71, a closed recirculation flow region is formed on the surface of the stator vane down stream of the obstruction without control, and the ZNMF jet actuator just reduces the extent of the recirculation region. Cross-stream distributions of the normalized cross-stream velocity component in the wake also indicated that the velocity deficit is reduced by the ZNMF jet actuator, and the downwash flow induced by the separation on the suction surface is also suppressed. So the lift of the stator increases, and the drag decreases, through which the ZNMF jet can balance the moment of the UAV. In a following study, Konor et al.[70] investigated the yaw angle of the UAV responses to the actuator activation in

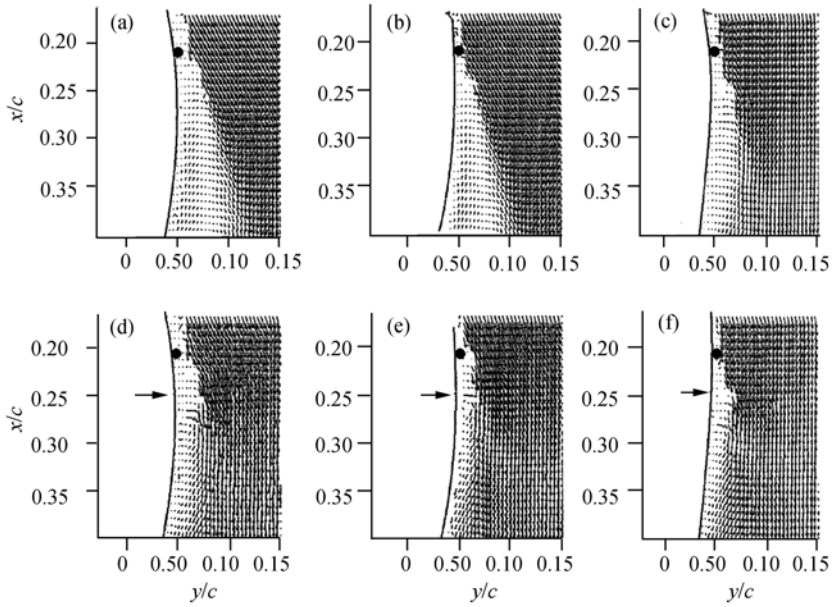

Figure 26 Velocity vector fields around the Clark-Y airfoil with an obstruction at x/c=0.21, the round speed 4300 r/min. Without control: (a) r/R=0.26, (b) 0.44, (c) 0.71; with control: (d), (e), (f)[69].

dynamic model fly tests. Comparing the time series of the yaw angle of the UAV with the actuator signal, they found that the yaw angle decreased to negative value since the actuator began to activate. As soon as the actuator activation turned off, the yaw angle started to increase. In this process, a definite delay in yaw angle action following actuator activation can be noted, which is most likely due to the aerodynamic lag in the inherent dynamics of the separation and reattachment process.

Recently, the research group supervised by Prof. Amitay investigated the vehicle control by the ZNMF jet flow control on the UAVs. The vehicle being used is a full-scale existing UAV platform nicknamed "Stingray" and based on the Air Force 1301 UAV design (Figure 27(a)). It is a blend wing body and controlled by four conventional flaps. The full scale model used in wind tunnel has a 2.8 m wing span and the leading edge swept angle of 50º. Washburn and Amitay[73] studied the active flow control enhanced aerodynamic performance of the full-scale Stingray UAV through experiments conducted in the NASA Langley Research Center transonic dynamics tunnel. The leading edge of each wing was instrumented with an array of ZNMF jet actuators, where the leading edge slot was divided into eight individually addressable sections. Each section was powered by 2 piezo-electric disks. The leading static pressure port in each row was at 40%, 62%, and 77% semi-span, respectively (Figure 27(b)). Forces and moments were acquired via an internal 6-component balance. The pressure distribution indicates that the ZNMF jet actuator will shift the suction peak forward towards the leading edge at the section with leading edge vortices, but has little influence on the pressure distribution in the section with leading edge vortices bursting and full separation of flow.

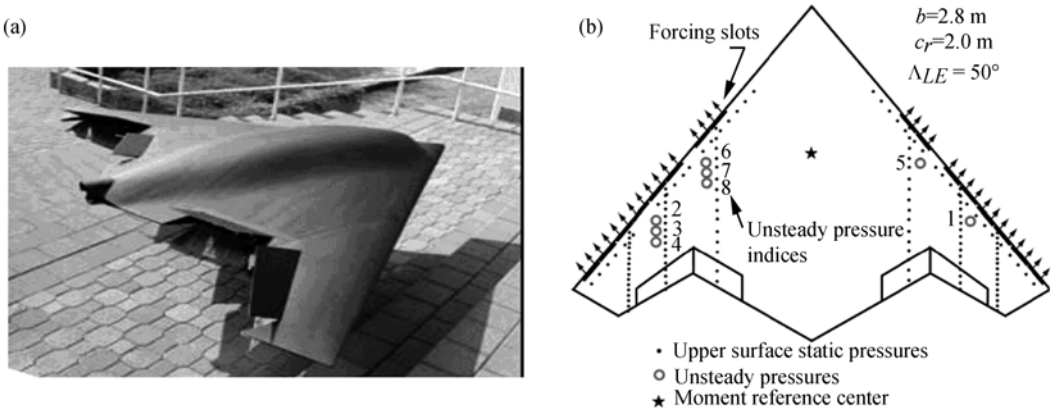

Figure 27 Stingray UAV. (a) The full scale model; (b) the model with ZNMF jet actuator and pressure sensor[74].

The lift, drag, rolling moment and pitching moment coefficients of the UAV controlled on one side of the wing varied with the actuator frequency are presented in Figure 28. Because the pressure distribution on the surface of the wing has little difference on the actuator activation, the changes in the lift and drag coefficients are very small. An increase of the lift coefficient by up to 4% and a decrease of 7% at high attack angle were found in the experiments, and the drag coefficient changes only 1% with respect to the baseline. However, these small lift and drag increments result in large variation of the pitch and roll moments as shown in Figurs 28(c) and 28(d). At higher angles of attack, as the actuator frequency is increased from low frequencies to high frequencies, the increment of rolling moment initially increases corresponding to increased suction on the port wing and opposite to the starboard flap effect. At each angle there is a critical actuator frequency, where

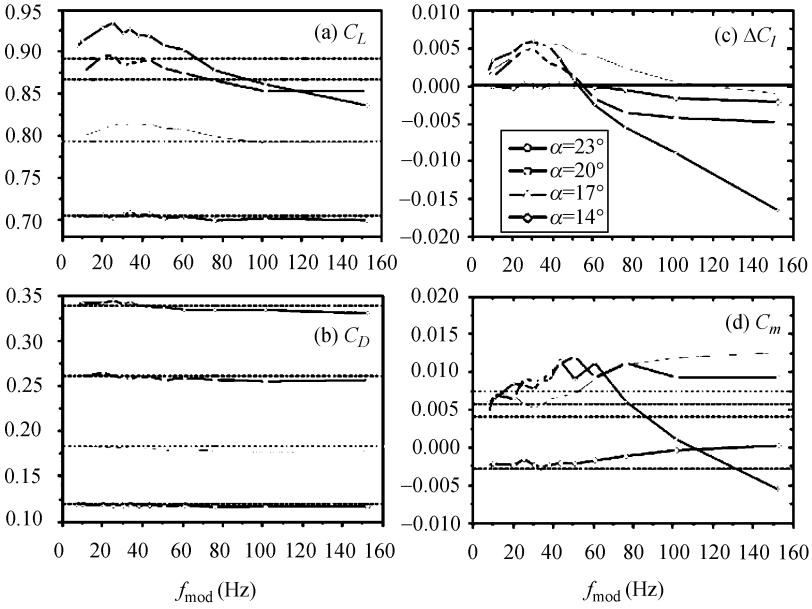

Figure 28 Aerodynamic forces and moments of Stingray UAV varied with the ZNMF jet actuator frequency[73].

the trend reverses (at α = 20°, and 23°, the increment of rolling moment becomes negative, i.e. below its baseline value without control). Therefore, the sign of the increment of rolling moment can be reversed merely by changing actuator frequency, which means the rolling moment of the UAV can be adjusted by changing the ZNMF jet actuator frequency, and the vehicle control could be obtained by using this active flow control method. The pitching moment with respect to the actuator frequency has similar trend to that of rolling moment. With the increase of attack angle, the efficiency of the flow controlled by the ZNMF jet on the UAV is enhanced, which is more attractive at high attack angles than the conventional passive flap.

Except for the open loop flow control on the MAV/UAV, Ciuryla et al.[75] carried out the experiments to investigate the close loop active stall suppression on the Cessna 182 UAV. Because the aerodynamic forces and moment associated with the stall cannot be measured during real flight, they used a dynamic shear stress sensor on the wingtips to detect the separation and the ZNMF jet actuators to reattach the flow. When the shear stress on the surface of the wing has a small value, the flow attaches to the wing surface. While the shear stress increases to some extent, the separation occurs and the ZNMF jet actuator should be initiated. Figure 29(a) presents a wing of Cessna 182 UAV model mounted with the dynamic shear stress sensor and the ZNMF jet actuator. In the close loop flow control experiments (see Figure 29(b)), with the increase of the attack angle, the shear stress begins to increase for flow separation. When the value of shear stress increases over the threshold value ($\mathrm{RMS}_{\mathrm{threshold}}$=0.5V), the ZNMF jet actuator is initiated and reattaches the flow to the wing surface, so the shear stress decreases immediately, and the rolling moment decreases too.

With the development of the research on the ZNMF jet flow control, this active flow control method begins to be applied to practical engineering. Air Force Research Laboratory, Lockheed Martin Aeronautics Company and General Electric Company were united to investigate the full scale flight demonstration of the ZNMF jet flow control on the pod wake in flight test[36]. The pod is a Low Altitude Navigation and Targeting Infrared for Night (LANTIRN) pod on the F-16 fighter.

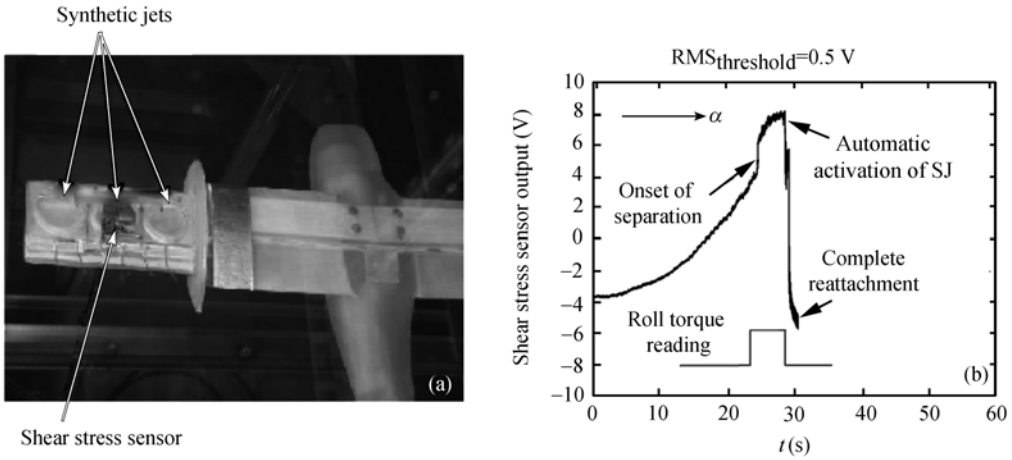

Figure 29 The close loop ZNMF jet flow control on the Cessna 182 UAV model. (a) The UAV model mounted with sensors; (b) the variation of shear stress with close loop control[75].

Two GE designed ZNMF jet actuators, known as PESJ, were used in this experiment. Each PESJ was connected to three holes, and each hole has an exit diameter of 3 mm. The actuators were run at 850 Hz and the hotwire velocity measurements conducted at the exit of each hole showed the peak values at the order of 250 m/s. Flight tests were conducted for Mach numbers from 0.4 to 0.85, altitudes from 5000 feet to 35000 feet, and various attack angles and yaw angles. The ventral fin of the F-16B fighter was instrumented with six dynamic pressure transducers, two accelerometers, and one strain gage to evaluate the fluctuate intensity of the pod wake (see Figure 30(a)). Figures 30(b)—30(d) show the level of suppression achieved under the specific test condition in which

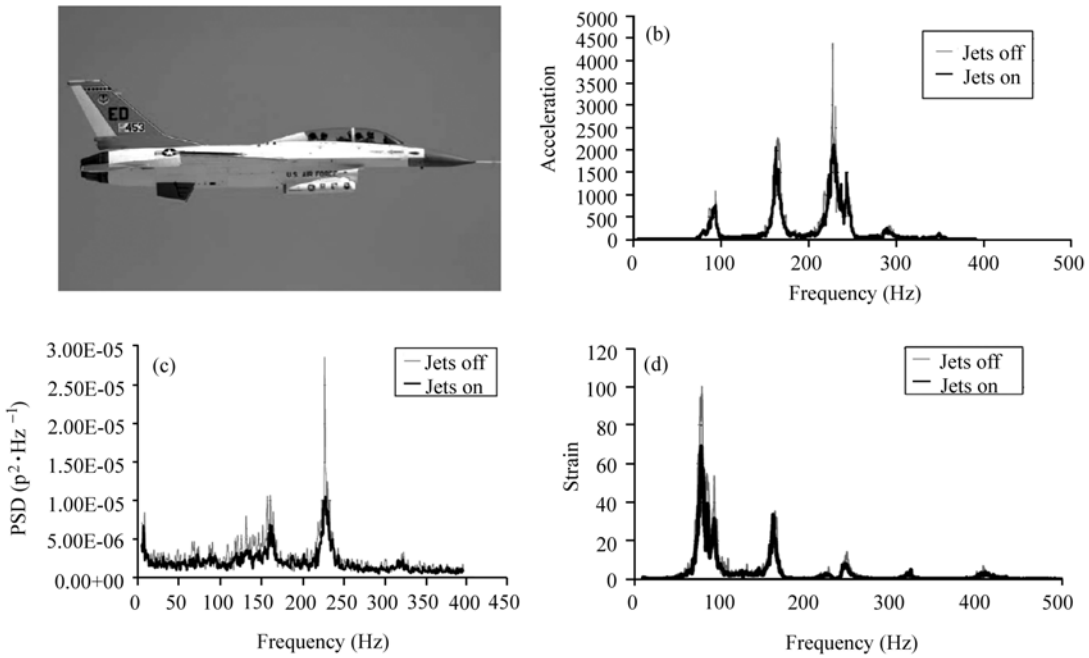

Figure 30 The flight test of ZNMF jet flow control on the LANTIRN pod wake of F-16 with Ma=0.5 and altitude 5000 feet. (a) F16 in flight test; (b) power spectrum of acceleration on the vertical pin; (c) the pressure fluctuation; (d) the shear stress[36].

suppression was realized with Ma=0.5 at 5000 feet altitude. All the three measurements demonstrated the effectiveness of the active flow control of the ZNMF jet, and the dynamic loads on the fin were suppressed, which resulted in the acceleration of the fin to be reduced and thus the strain levels at the mounting location were also reduced. It is prudent to assume that the fin, or any other structure located down stream of the pod, would have an increased mean time to fail with these reductions.

5 Conclusions

In the last 50 years, there has been much improvement on the communication, navigation and electrical vehicle control systems in modern aircrafts, but the flow control always uses the conventional ailerons, spoilers and flaps. With the demands on revolutionized aviation associated with the environmental and cost requirements, lighter and more compact flow control concepts and technologies are underway to introduce changes in aircraft designs that will reduce acoustic loads, total vehicle drag and emissions while increasing the system transport capacities, safety, endurance and range. Even though the suggested innovations may be drastic, risky and costly, the future of the aviation industry relies heavily on ground-breaking research areas such as active flow control. The ZNMF jet flow control is a novel active flow control method integrated with the advanced material, electro-mechanical and manufactory techniques. The actuator based on the piezoelectricity can have larger blowing velocity with small power input by using Helmholtz resonance in the cavity, so it is possible for this flow control method to be used in practical engineering. Meanwhile, the development of the MEMS will result in the high compact, micro, high efficient, robust and low cost ZNMF jet actuators, which have wide applications for the flow control in aviation including MAV and UAV.

Although the ZNMF jet flow control method has much improvement compared with those in last decade, there always remain a lot of issues lacking uniform conclusion, such as the influence of key parameters on the flow structure and the flow control efficiency. The most accepted key parameters at present are the stroke length ratio and the Reynolds number based on the time averaged blowing velocity, which determines the strength and trajectory of the vortex pair or ring. The other parameters, such as the geometry of the actuator cavity, the width to thickness ratio of the orifice, the geometry of the orifice, Strouhal number and Stokes number of the actuator, also have much influence on the vortex pair or ring formation and evolution. For example, Wu and Breuer[76] figured out that Stokes number represents the ratio of orifice diameter to the boundary layer thickness in the orifice ($\delta_v^2 = v/w$, $S^2 = wD_0/v = D_0/\delta_v$). If Stokes number is small, the viscous effect should be taken care, otherwise the fluid will be blocked near the orifice. Zhong et al.[26] concluded a minimum Stokes number of about 10 is required for an appreciable rollup to occur. In the applications of the ZNMF jet, except for the different conclusions about the mechanism, the optimum actuator frequency and location, there is no general conclusion for the key parameter to represent the strength of the jets with respect to the incoming flow. The velocity ratio $R = U_0/U_\infty$ is commonly adopted in literature, but the momentum coefficient C_μ represents the momentum flux of the jets relative to the incoming flow, which contains not only the velocity ratio of the jet to the incoming flow but also the ratio of the actuator orifice scale to the scale of the controlled body. So the effect of the momentum coefficient on the flow structure produced by the ZNMF jet is different from that of the velocity ratio. These issues should be carefully investigated in order to apply the ZNMF jet

flow control in practical engineering.

Beside the issues in fluid mechanics, more attention should be paid to the research and maintenance of the actuator itself. The widely used ZNMF jet actuator is manufactured by piezoelectricity. The principle of this kind of actuator is that it should be worked as the structure resonance frequency or the cavity Helmholtz frequency to achieve high efficiency, which will lead to the structure fatigue. However, in practical applications, it is expected that the ZNMF jet actuator has a wide range of working frequency and a long working life. Meanwhile, the development of the MAV and the micro fluid requires the micro and high compact actuator, which relies on the development of the material, electro-mechanical and manufacturing technology. For the maintenance of the actuator, similar to other blowing or suction active flow control methods, the risk of ingesting dust will block the orifice, which will decrease the efficiency of the actuator, even make the actuator invalid. So the research about the cleaning technique for the actuator or the self cleaned actuator is also important for the application of the ZNMF jet flow control.

The authors would like to thank Prof. D.R Smith. of Wyoming University and Prof. S. Zhong of University of Manchester for the discussion during the manuscript preparation.

1 Ingard U, Labate S. Acoustic circulation effects and the nonlinear impedance of orifices. J Acoust Soc Am, 22(2): 211－218
2 Ming X, Dai C Y, Shi S X. A new phenomenon of acoustic streaming. Acta Mech Sin (in Chinese), 1992, 24(1): 48－54
3 Wiltse J, Glezer A. Manipulation of free shear flows using piezoelectric actuators. J Fluid Mech, 1993, 249: 261－285
4 Luo Z B, Xia Z X. Advances in synthetic jet technology and applications in flow control. Adv Mech (in Chinese), 2005, 35(2): 221－234
5 Luo Z B, Xia Z X, Liu B. New generation of synthetic jet actuators. AIAA J, 2006, 44(10): 2418－2420
6 Luo Z B, Xia Z X. A novel valve-less synthetic-jet-based micro-pump. Sensor Actuat A-Phys, 2005, 122(1): 131－140
7 Zhang P F, Wang J J. Novel signal wave pattern to generate more efficient synthetic jet. AIAA J, 2007, 45(5): 1058－1065
8 Wang J J, Feng L H, Xu C J. Experimental investigations on separation control and flow structure around a circular cylinder with synthetic jet. Sci China Ser E-Tech Sci, 2007, 50(5): 550－559
9 Feng L H, Wang J J, Xu C J. Experimental verification of a novel actuator signal for efficient synthetic jet. J Exp Fluid Mech (in Chinese), 2007, 22(1): 6－10
10 Liu Y M, Wu N M, Dong J Z, et al. Process mechanism of synthetic jet and its effect on the mixing in coaxial jets. J Beihang University (in Chinese), 2007, 33(1): 5－9
11 Zhao H, Yang Z G, Lou H J. Experimental investigation of flow characteristics of synthetic jet and it's preliminary application to combustion. J Aerospace Power (in Chinese), 2004, 19(4): 512－519
12 Sun J H, Ji Y M, Ming X, et al. Gas oscillations in open pipes and application in atomization. Acta Aerodync Sin (in Chinese), 1997, 15(2): 177－184
13 Sun J H, Ming X. Effect of nonlinear gas oscillations on wing-tip vortexes. J Nanjing Univ Aeronaut Astronaut (in Chinese), 2004, 36(1): 39－43
14 Zhang F Y, Li L, Dong Y, et al. Experimental investigation of flow vectoring by using zero-mass synthetic jets actuator. J Propulsion Tech (in Chinese), 2004, 25(3): 224－226
15 Hao L S, Qiao Z D. Maximizing the effect of synthetic jet on airfoil separation flow control. J Northwestern Polytech Univ (in Chinese), 2006, 26(4): 528－531
16 Gao F, Wang L. Numerical study on synthetic flow field of adjacent microjet actuators. Acta Aerodync Sin (in Chinese), 2003, 21(3): 267－274
17 Luo X B, Li Z X, Guo Z Y. Analysis of the mechanism of synthetic jet formation. J Tsinghua Univ (Sci Tech)(in Chinese), 2000, 40(12): 24－28
18 Luo X B, Li Z X, Guo Z Y. Numerical simulations on flow field of incompressible synthetic jet. J Eng Thermophys (in Chinese), 2001, 22: 56－58
19 Glezer A, Amitay M. Synthetic jets. Annu Rev Fluid Mech, 2002, 34: 503－529
20 Kiddy J, Chen P, Niemczuk J, et al. Active flow control using micro electro-mechanical systems. AIAA Paper 2000-1561,

2000
21 Glezer A, Amitay M, Honohan A. Aspects of low and high frequency actuation for aerodynamic flow control. AIAA J, 2005, 43(7): 1501－1511
22 Smith B L, Glezer A. The formation and evolution of synthetic jets. Phys Fluids, 1998, 10(9): 2281－2297
23 Glezer A. The formation of vortex rings. Phys Fluids, 1988, 31(12): 3532－3541
24 Zhong S, Jabbal M, Tang H, et al. Toward the design of synthetic jet actuators for full scale Flight conditions, Part 1: the fluid mechanics of synthetic jet actuators, Flow, Turbulence and Combustion, 2007, 78: 283－307
25 Utturkar Y, Holman R, Mittal R. A jet formation criterion for synthetic jet actuator. AIAA Paper 2003-0636, 2003
26 Holman R, Utturkar Y, Mittal R, et al. A formation criterion for synthetic jets. AIAA J, 2005, 43(10): 2110－2116
27 Shuster J.M, Smith D R. Experimental study of the formation and scaling of a round synthetic jet. Phys Fluids, 2007, 19(4): 045109-045109-21
28 Smith B L, Swift G W. Synthetic jet at large Reynolds number and comparison to continuous jets. AIAA Paper 2001-3030, 2003
29 Gharib M, Rambod E, Shariff K. A universal time scale for vortex ring formation. J Fluid Mech, 1998, 360: 121－140
30 Smith B L, Glezer A. Vectoring and small scale motions effected in free shear flows using synthetic jet actuators. AIAA Paper 97-0213, 1997
31 James R D, Jacobs J W. A round turbulent jet produced by an oscillating diaphragm. Phys Fluids, 1996, 8(9): 2484－2495
32 Gordon M, Cater J E, Soria J. Investigation of the mean passive scalar field in zero-net-mass-flux jets in cross-flow using planar laser induced florescence. Phys Fluids, 2004, 16(3): 794－808
33 Hassan A, Munts E. Transverse and near tangent synthetic jets for aerodynamic flow control. AIAA Paper 2000-4334, 2000
34 Duvigneau R, Visonneau M. Simulation and optimization of stall control using a synthetic jet, AIAA paper 2004-2315, 2004
35 Smith D, Amitay M, Glezer A. Modification of lifting body aerodynamics using synthetic jet actuators. AIAA Paper 98-0209, 1998
36 Shaw L, Smith B, Saddoughi S. Full scale flight demonstration of active flow control of a pod wake. AIAA Paper 2006-3183, 2006
37 Rumsey C L, Gatski T B, Sellers W L. Summary of the 2004 CFD validation workshop on synthetic jets and turbulent separation control, AIAA Paper 20004-2217, 2004
38 Milanovic I, Zaman M, Rumsey C. An Isolated circular synthetic jet in cross-flow at low momentum-flux ratio. AIAA Paper AIAA 2005-1110, 2005
39 Schaeffler N. The isolated synthetic jet in cross-flow: a benchmark for flow control simulation. AIAA Paper 2004-2219, 2004
40 Rumsey C. Computation of a synthetic jet in a turbulent cross-flow boundary layer. NASA/TM-2004-213273, 2004
41 Schaeffler N. The interaction of a synthetic jet and a turbulent boundary layer. AIAA Paper 2003-643, 2003
42 Keffer J F, Baines W D. The round turbulent jet in a cross-wind. J FluidD Mech, 1963, 15: 481－496
43 Pratte B D, Baines W D. Profiles of the round turbulent jet in a cross flow. J Hydraulic Division, Am Soc Civil Eng, 1967, 92(2): 53－64
44 Smith S H, Mungal M G. Mixing, structure and scaling of the jet in crossflow. J Fluid Mech, 1998, 357: 83－122
45 Hasselbrink E F, Mungal M G. An analysis of the time-averaged properties of the far field of the transverse jet. AIAA Paper 96-0201, 1996
46 Ugrina S. Experimental analysis and analytical modeling of synthetic jet cross flow interaction. Ph.D Dissertation. Maryland: University of Maryland, 2007
47 Mittal R, Rampunggoon P. Interaction of synthetic jet with a flat plate boundary layer. AIAA Paper 01-31243, 2001
48 Mittal R, Rampunggoon P. On the virtual aeroshaping effect of synthetic jets. Phys Fluids, 2002, 14(4): 1533－1536
49 Crook A, Wood N J. Measurements and visualization of synthetic jets. AIAA Paper 2001-0145, 2001
50 Amitay M, Honohan A M, Trautman M, et al. Modification of the aerodynamic characteristics of bluff bodies using fluidic actuators. AIAA Paper 97-2004, 1997
51 Honohan A.M, Amitay M, Glezer A. Aerodynamic Control Using Synthetic Jets. AIAA Paper 2000-2401, 2000
52 Catalanoy P, Wang M, Iaccarino G, et al. Optimization of cylinder flow control via actuators with zero net mass flux. Centre for Turbulence Research, Proceedings of the Summer Program. NASA Ames/Stanford University, CA, 2007. 297－304
53 Smith D R, Amitay M, Valdis K, et al. Modification of lifting body aerodynamics using synthetic jet actuators. AIAA Paper 98-0209, 1998

54 Amitay M, Smith D R, Kibens V, et al. Aerodynamic flow control over an unconventional airfoil using synthetic jet actuators. AIAA J, 2001, 39(3): 361－370
55 Amitay M, Glezer A. Role of actuation frequency in controlled flow reattachment over a stalled airfoil. AIAA J, 2002, 40(2): 209－216
56 Zhang P F, Wang J J. Numerical simulation on flow control of stalled NACA0015 airfoil with synthetic jet actuator in recirculation region. J Beihang Univ (in Chinese), 2008, 34(4): 443－446
57 Gilarranz, J, Traub L, Rediniotis O. Characterization of a compact, high power synthetic jet actuator flow separation control. AIAA Paper 2002-0127, 2002
58 Seifert A, Darabi A, Wygnanski I. Delay of airfoil stall by periodic excitation. AIAA J, 1996, 33(4): 691－707
59 Ravindran S S. Active control of flow separation over an airfoil. NASA/TM-1999-209838, 1999
60 Tuck A, Soria J. Separation control on a NACA 0015 airfoil using a 2D micro ZNMF. Aircraft Eng Aerospace Technol, 2008, 28(2): 175－180
61 Donovan J F, Kral L D, Cary A W. Active flow control applied to an airfoil. AIAA Paper 98-0210, 1998
62 Milanovic I M, Zaman K. Highly inclined jets in cross-flow. AIAA Paper 2003-0183, 2003
63 Zhong S, Garcillan L, Wood N J. Dye visualisation of inclined and skewed synthetic jets in a cross-flow. Aeronaut J, 2005, 109(2): 147－155
64 Seifert A, Pack L. Separation control at flight Reynolds numbers – lessons learned and future directions. AIAA Paper 2000-2542, 2000
65 Suzuki T. Effect of a synthetic jet acting on a separated flow over a hump. J Fluid Mech, 2007, 547: 331－359
66 Dandois J, Garnier E, Sagaut P. Numerical simulation of active separation control by a synthetic jet. J Fluid Mech, 2007, 574: 25－58
67 Brunn A, Nitsche W. Active control of turbulent separated flows over slanted surfaces. Int J Heat Fluid FL, 2006, 27: 748－755
68 Parviz B A, Najafi K, Muller M O, et al. Electrostatically driven synthetic microjet arrays as a propulsion method for micro flight, Part II: microfabrication and initial characterization. Microsyst Technol, 2005, 11: 1292－1300
69 Fung P, Amitay M. Control of a miniducted-fan unmanned aerial vehicle using active flow control. J Aircraft, 2002, 39(4): 561－571
70 Kondor S, Amitay M, Parekh D, et al. Active flow control application on a mini ducted fan UAV. AIAA Paper 2001-2440, 2001
71 Chatlynne E, Rumigny N, Amitay M, et al. Virtual aero shaping of a Clark-Y airfoil using synthetic jet actuators. AIAA Paper 2001-0732, 2001
72 Amitay M, Horvath M, Michaux M, et al. Virtual aerodynamic shape modification at low angles of attack using synthetic jet actuators. AIAA Paper 2001-2975, 2001
73 Washburn A E, Amitay M. Active flow control on the Stingray UAV: physical mechanisms. AIAA Paper 2004-0745, 2004
74 Amitay M, Parekh D E. Active flow control on the Stingray uninhabited air vehicle: transient behavior. AIAA J, 2004, 42(11): 2205－2215
75 Ciuryla M, Liu Y, Farnsworth J, et al. Flow control and flight control on a Cessna 182 model. J Aircraft, 2007, 44(2): 653
76 Wu K E, Breuer K S. Dynamics of synthetic jet actuator arrays for flow control. AIAA Paper 2003-4257, 2003